

# Mach bands and multiscale models of spatial vision: The role of first, second, and third derivative operators in encoding bars and edges

Stuart A. Wallis

School of Life and Health Sciences, Aston University,  
Birmingham, UK



Mark A. Georgeson

School of Life and Health Sciences, Aston University,  
Birmingham, UK



Ernst Mach observed that light or dark bands could be seen at abrupt changes of luminance gradient in the absence of peaks or troughs in luminance. Many models of feature detection share the idea that bars, lines, and Mach bands are found at peaks and troughs in the output of even-symmetric spatial filters. Our experiments assessed the appearance of Mach bands (position and width) and the probability of seeing them on a novel set of generalized Gaussian edges. Mach band probability was mainly determined by the shape of the luminance profile and increased with the sharpness of its corners, controlled by a single parameter ( $n$ ). Doubling or halving the size of the images had no significant effect. Variations in contrast (20%–80%) and duration (50–300 ms) had relatively minor effects. These results rule out the idea that Mach bands depend simply on the amplitude of the second derivative, but a multiscale model, based on Gaussian-smoothed first- and second-derivative filtering, can account accurately for the probability and perceived spatial layout of the bands. A key idea is that Mach band visibility depends on the ratio of second- to first-derivative responses at peaks in the second-derivative scale-space map. This ratio is approximately scale-invariant and increases with the sharpness of the corners of the luminance ramp, as observed. The edges of Mach bands pose a surprisingly difficult challenge for models of edge detection, but a nonlinear third-derivative operation is shown to predict the locations of Mach band edges strikingly well. Mach bands thus shed new light on the role of multiscale filtering systems in feature coding.

Keywords: human vision, Mach bands, psychophysics, feature detection, edges, bars, scale-space, Gaussian derivatives, even and odd filters

Citation: Wallis, S. A., & Georgeson, M. A. (2012). Mach bands and multiscale models of spatial vision: The role of first, second, and third derivative operators in encoding bars and edges. *Journal of Vision*, 12(13):18, 1–25, <http://www.journalofvision.org/12/13/18>, doi:10.1167/12.13.18.

## Introduction

### Mach bands

In the 1860s Ernst Mach observed that illusory light (or dark) bars or bands could be seen in the absence of corresponding peaks (or troughs) in luminance. The phenomenon has come to be known as *Mach bands*, though Weale (1979) argued that the bands were almost certainly known to artists of the 15<sup>th</sup> century Italian Renaissance. The bands are typically seen at abrupt changes of luminance gradient, such as the junction of a luminance ramp and a plateau—a luminance profile often known as the *Mach ramp*. Importantly for theories of visual feature detection (Morgan, 2011), the existence of Mach bands shows that not all perceived bars or lines arise from peaks or troughs in the luminance profile. Given its long history, it is not surprising that quite a number of models and theories

of the Mach phenomenon have been proposed (Pessoa, 1996). Though they differ in scope and detail, one central idea—spatial filtering by even-symmetric, center-surround receptive fields—is common to all models, including MIRAGE (Morgan & Watt, 1997; Watt & Morgan, 1985) and the local energy model (Ross, Morrone & Burr, 1989). A long-standing difficulty has been in constructing a broader theory that embeds this filtering into a satisfactory, more general theory of spatial vision. Our aims in this paper are (a) to describe a multiscale model for visual (1-D) feature detection based on earlier models of edge coding (Georgeson, May, Freeman, & Hesse, 2007), extended to deal with both even- and odd-symmetric features (bars and edges) in an integrated fashion and (b) to apply this model to new experimental data on the perceived structure of Mach bands and the probability of reporting them under different conditions.

With great prescience, Mach (1865) formulated a mathematical expression for brightness that would

explain the band phenomenon, proposing that the bands were seen at peaks and troughs in the second derivative of the luminance profile, and he conjectured that this might be implemented by reciprocal interaction of neighboring retinal cells. As a result, light (or dark) bands would be seen when the luminance at one location was higher (or lower) than the average of its neighbors: “Whatever is near the mean of the surroundings becomes effaced; whatever is above or below is disproportionately brought into prominence” (Mach, 1865; see Ratliff, 1965, p. 306). Several early studies concluded that Mach bands were seen at or near the peaks and troughs in the second derivative of the luminance profile (Burnham & Jackson, 1955; Charman & Watrasiewicz, 1964; Ludvigh, 1953a, 1953b; O’Brien, 1958; Thomas, 1965). Put simply, the bands might occur at points of maximum curvature in the luminance profile, even when those points are not peaks or troughs of luminance. However, the stimuli in those early experiments were difficult to control, and the evidence was not extensive. Our goal here is to provide a more systematic account of the way Mach bands depend on the spatial scale and shape of the luminance waveform and to develop a computational model for bar and edge features, based on Gaussian-derivative filtering that can account accurately for the perceived structure of the bands and the probability of seeing them. We collected data on the perceived position of the bands and the perceived position of the edges of the bands. We shall see that the edges of Mach bands pose an interesting challenge to models of feature detection. The experiments and model thus focus on the type and location of elementary features seen and do not address questions about perceived contrast or brightness of the bands. For an extensive review of early models and data and translations of Mach’s six key papers, see Ratliff (1965) and for a more recent review, see Pessoa (1996).

### A note on terminology: Scale, blur, gradient, derivative, Gaussian derivative

The terms *scale* and *derivative* are used extensively in this paper, and we use them in several contexts that should not be confused.

Scale here refers to “size” or “spatial extent” (not “axis” or “dimension”). In the experiments we use edge images that have a certain scale (the luminance transition occurs over a given spatial extent), defined by a scale parameter  $\sigma$ . Doubling or halving  $\sigma$  alters their size or scale accordingly. But the spatial filters applied to these images also have a range of sizes or filter scales  $s$ ; doubling or halving  $s$  shifts the filter by one octave towards lower or higher spatial frequencies. Importantly, when an image is spatially filtered at multiple scales (a multiscale filter system), then the response to a single

stimulus of scale  $\sigma$  is distributed over many filter scales ( $s$ ) and over space ( $x$ ). The 2-D distribution of responses over ( $x, s$ ) is a *scale-space map*. (For a wide-ranging account of the scale-space approach to biological and computer vision, see ter Haar Romeny, 2003, and for more mathematical detail, see Lindeberg, 1994.)

*Blur* is a simple form of low-pass spatial filtering, in which the image is smoothed by convolution with a (usually) unimodal blur kernel or point-spread function. In Gaussian blur, the kernel is a Gaussian function  $G(x, b)$  of unit area (in 1-D) or unit volume (in 2-D). The degree of blurring is controlled by the scale parameter or blur  $b$ .

The *gradient* profile of a 1-D image whose luminance profile is  $L(x)$  is its first derivative  $L'(x)$  or  $dL/dx$  defined in the usual way. It measures the slope of the function at each point  $x$ —the change  $\delta L$  in  $L$  over an infinitesimal distance  $\delta x$ . The second derivative is the gradient of the gradient,  $d^2L/dx^2$  equal to  $dL'/dx$ . It is closely related to local curvature in  $L(x)$ .

If we blur an image and compute its gradient profile, these two linear operations can be lumped together as one: We have calculated the smoothed derivative of the image. Which operation comes first is immaterial. For a noisy signal, the smoothing combats high frequency noise that is amplified by differentiation. When the smoothing is Gaussian, with scale  $s$ , the combined operation is the *Gaussian derivative* and the filter kernel is  $dG(x, s)/dx$ , sketched at the top of Figure 1D. In the absence of nonlinearity, several blurring and derivative operations can be chained (in any order) to create higher order Gaussian derivatives. Gaussian-derivative filters are spatial frequency tuned filters whose bandwidth decreases as the derivative order (first, second, etc.) increases. Peak spatial frequency is inversely proportional to filter scale  $s$ . Receptive field symmetry matches the derivative order: odd orders (1, 3, 5...) have odd symmetry; even orders (2, 4, 6...) have even symmetry. In this paper we consider mainly the first (odd) and second (even) Gaussian derivatives. If we blur an image with Gaussian blur  $b$  and compute its Gaussian derivative at scale  $s$ , the blurring and smoothing simply combine quadratically,  $s' = \sqrt{b^2 + s^2}$ , and the outcome is exactly equivalent to applying a Gaussian derivative with a larger scale  $s'$ . Because of this quadratic relation, small input blurs  $b$  have little influence at large filter scales, that is  $s' \approx s$ , if  $b \ll s$ .

Thus in this paper when we refer simply to derivatives of the image we mean the pure mathematical (infinitesimal) derivative, but when we refer to smoothed derivatives, derivative filters, or multiscale derivatives we mean Gaussian first (or higher) derivatives at one or more scales  $s$ . We try to distinguish clearly between stimulus scale ( $\sigma$ ) and filter scale ( $s$ ). In particular, the scale  $s$  of the most active filter can vary with the shape of the waveform as well as the stimulus scale parameter  $\sigma$ .

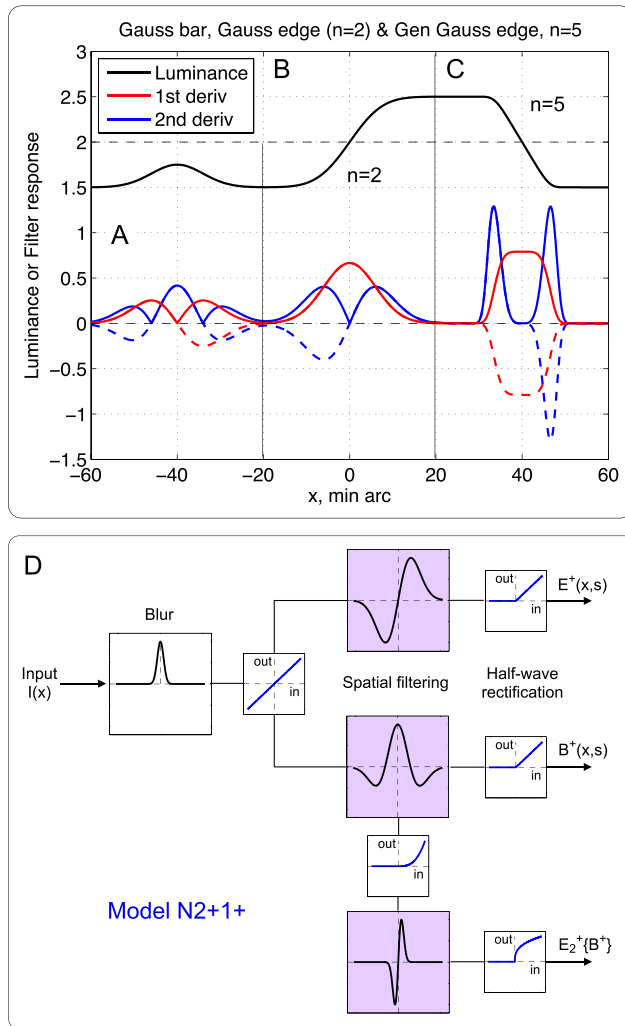


Figure 1. A, B, and C: Three luminance waveforms (black curves) and their first (red) and second (blue) spatial derivatives computed at high pixel resolution to approximate the mathematical (infinitesimal) derivative. Dashed curves show the negative parts of each function while solid curves show the magnitude or absolute value. Amplitudes of the derivatives have been arbitrarily scaled (same scaling for A, B, and C) to illustrate our general idea that the gradient response (red curve) might occlude the perception of bars given by peaks in the second derivative in some cases (A, B) but not others (C). A: Gaussian bar; B: Gaussian edge; C: generalized Gaussian edge that is more like a Mach ramp with exponent  $n = 5$  (see [Methods](#)). D: Sketch of the signal-processing model developed in this paper, based on multiscale Gaussian derivative filters. Basic model (dubbed N2+1+) contains odd- and even-symmetric receptive fields (RFs; shaded boxes) whose outputs are half-wave rectified to give response maps (scale-space maps)  $E^+(x, s)$ ,  $B^+(x, s)$  that are a function of RF position ( $x$ ) and scale ( $s$ ). Channels of opposite polarity ( $E^-$ ,  $B^-$ ) are also needed. The model reports Mach bands at response peaks in  $B^+$  or  $B^-$  if the B/E response ratio exceeds a criterion value. A third type of output channel ( $E_2$ ) was added to account for the perceived edges of Mach bands.

## Mach bands and spatial derivatives

Figure 1 shows luminance profiles (black curves) for (A) a Gaussian bar, (B) a Gaussian-blurred edge, and (C) an edge that is more like a Mach ramp (defined more precisely later). Also shown are the corresponding first and second derivative profiles, computed numerically with high pixel resolution. As expected, the second derivative (blue) shows peaks at points of high curvature in the luminance profile—the center of the bar (A) and the corners of the edge profiles (B and C). Notice how at the corner points, the second derivative amplitude increases markedly when the edge is made more ramp-like (Figure 1C), making the corners sharper. Points of high curvature in the luminance profile may represent key features in the image, and so the strength of Mach bands might depend directly on the amplitude of the second derivative peaks. But if that were so, then we should expect Mach bands to have several interesting properties: (a) Mach band strength should increase with contrast, because the derivative amplitudes of any order (first, second, etc.) are directly proportional to contrast; (b) Mach band strength should be markedly greater when images are scaled down in size, because there is an inverse-square relation between second derivative amplitude and scale. While the first derivative amplitude doubles, the second derivative amplitude quadruples every time the ramp width is halved. (c) Comparing the blue peaks in Figure 1B and C, we should expect Mach bands to be stronger at sharper corners. Our experiments shed light on these expectations, and we confirm item (c) but find no evidence to support item (b) and no general support for item (a), thus raising the question of what a more suitable model should be like.

One observation that motivated our approach was that Mach bands on Gaussian edges seemed rather weak (and apparently passed unnoticed in an earlier study; Hesse & Georgeson, 2005), while the corresponding peaks and troughs in the second derivative are substantial (Figure 1B). We shall suggest that a general solution lies in the combination of two main ideas—multiscale spatial filtering and a suitable comparison of the outputs of even- and odd-symmetric filters to derive the type and location of features in the image. These elements exist in previous models, but a novel combination of them—briefly outlined next—appears promising and fruitful.

## Multiscale detection of bars and edges

In developing models for feature detection in machine vision and building on the pioneering work of Koenderink (1984) and Koenderink and van Doorn (1987), Lindeberg (1998) showed elegantly how, for any

given feature such as a blurred bar, blob, or edge, the amplitudes (gains) of a set of multiscale Gaussian derivative filters of suitable order (first, second, third. . .) could be chosen a priori to ensure that a peak response over filter scales would always occur in the filter whose scale equals that of the image feature in question. Thus, in Lindeberg's terminology, one can use *scale normalization* (the setting of filter gains) to achieve automatic, image-driven *scale selection*. This peak-finding scheme can identify the location, scale, and identity of image features—a crucial step in early visual coding. Georgeson et al. (2007) showed how these principles could be used to model the process of localizing blurred edges and encoding edge blur in human vision. They evaluated two models called N1+ and N3+ that used multiscale first- and third-derivatives, respectively. (Note: N denotes use of Lindeberg's scale-normalization; one or three indicates the order of derivatives used; + indicates the use of half-wave rectification on the output of the filters.) In the present paper we describe how this approach via Gaussian derivatives in scale-space can be extended to encode both bars and edges using even- and odd-symmetric filters, respectively (Figure 1D; described in detail later). We suggest that these filters do not act as independent channels, nor are their responses combined (as in the local energy model; Morrone & Burr, 1988; Ross et al., 1989), nor do they act competitively. Rather, it is a comparison of the even and odd filter responses that enables a decision about feature presence or absence. Such a comparison also formed part of the local energy model where it was used to evaluate local phase and classify energy peaks as either bars or edges. Here we make no use of the energy measure because it is (by definition) the smooth spatial envelope of the even and odd responses, and that turns out to exclude too many features that are actually perceived (Hesse & Georgeson, 2005).

Our concept of the even/odd comparison is illustrated in Figure 1B and 1C. The solid blue curve shows the magnitude of the second derivative (the bar response), while the solid red curve shows the first derivative (gradient magnitude, a possible edge response), with arbitrary relative scaling of the two curves. In brief, our proposal is that a bar is seen at locations where (a) the bar response is a local maximum and (b) that response exceeds the edge response at the same location by a sufficient amount that depends on internal noise and on the observer's criterion. Thus, in Figure 1B and 1C, Mach bands might be more likely on the ramp edge (C) than the Gaussian edge (B) not simply because the bar responses are larger, but because the ratio of bar-to-edge response is larger at the bar response peaks. Put another way, we can say that the Mach bands on a Gaussian edge are largely occluded by the edge response but on the ramp edge they are not.

## The present experiments

As part of our effort to understand how multiscale spatial filtering serves to encode local features (Georgeson et al., 2007; Hesse & Georgeson, 2005; Wallis & Georgeson, 2009), we here examine how the perception of bars (Mach bands) is affected by the nature of the transition from the ramp region to the plateau region. We introduced a stimulus manipulation that changes the curvature of the luminance profile at the ramp-plateau junction. Since second derivative amplitude is a measure of curvature (see above), we might expect this manipulation to affect the probability of seeing Mach bands. The luminance waveform was the cumulative integral of a *generalized Gaussian* profile (described below). In Experiments 1 and 3 we used the yes-no method to evaluate the probability of reporting Mach bands, and in Experiment 2 we used the feature-marking method (Georgeson & Freeman, 1997) to assess the geometry of Mach bands by marking both the center positions of the bands and the edges of the bands.

## Methods

### Stimulus design

Luminance profiles  $L(x)$  of the vertical 1-D images could vary from a Mach ramp through to a Gaussian edge and beyond under the control of a single shape parameter  $n$ . Their first derivative (gradient) profile was defined as a generalized Gaussian function (Figure 2A)

$$\frac{dL}{dx} = A_n \exp\left(\frac{-|x|^n}{2\sigma^n}\right), \quad (1)$$

where  $n = 1, 1.5, 2, 2.5, 3, 4, \text{ or } 5$ , and  $A_n$  is a constant that controls the gradient magnitude and contrast of the image. When  $n = 2$  the first derivative was a Gaussian. Each waveform was sampled at 1 min arc intervals and integrated numerically using the *cumtrapz* function in Matlab and scaled to a common amplitude to form the luminance profile of a blurred vertical dark-to-light edge (Figure 2B). A copy of each waveform was left-right reversed to form a light-to-dark edge. Edges of different scales were obtained by setting  $\sigma = 3, 6, \text{ or } 12$  min arc. Increases (or decreases) of  $n$  sharpen (or blur) the upper and lower corners of the waveform as shown in Figure 2B. Thus the family of luminance waveforms ranged from a very smooth profile ( $n = 1$ ; Figure 2C) through the Gaussian integral ( $n = 2$ ), to a slightly blurred Mach ramp ( $n = 5$ ; Figure 2D).

Figure 3A illustrates the family of luminance waveforms (for  $n = 1, 2, 3, \text{ and } 5$ ) at the three scales

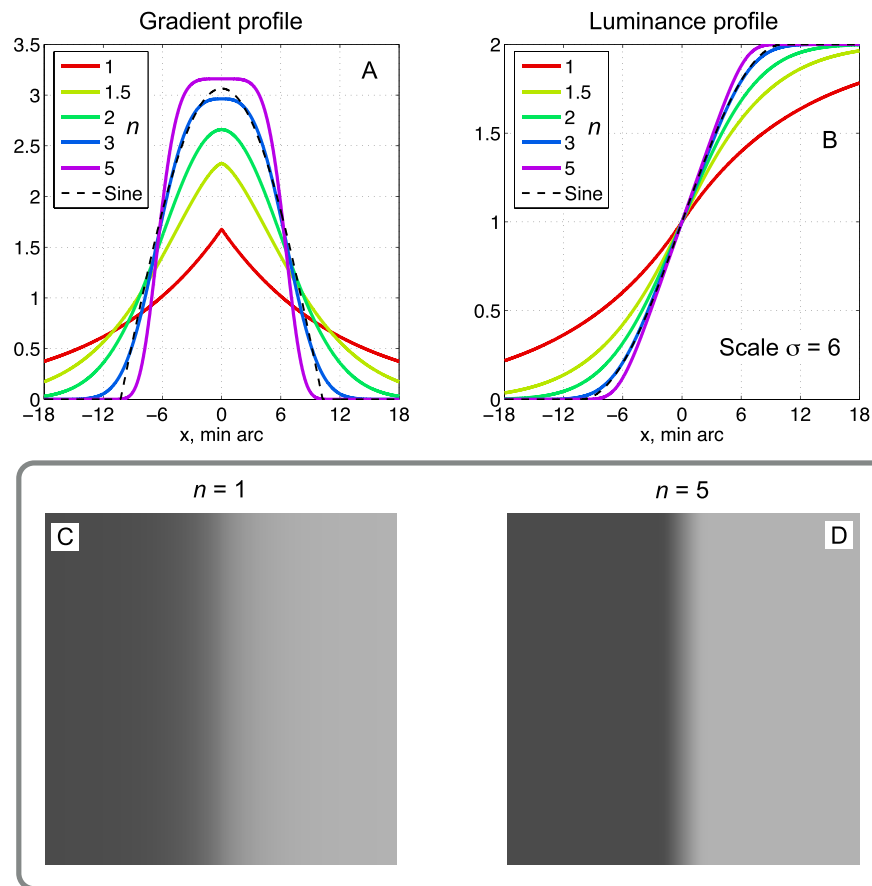


Figure 2. Constructing the stimuli. Generalized Gaussian functions (A) were integrated numerically to produce the edge profiles (B). The shape (kurtosis; peakiness) of the gradient profiles (A) is controlled by the exponent ( $n$ ) in Equation 1 independently of spatial scale  $\sigma$ . Varying  $n$  allows one to move smoothly from the Gaussian edge ( $n = 2$ ) to the Mach ramp ( $n$  high). Only dark-to-light edges are shown here but both polarities were used. Luminance profiles were scaled to have the same contrast; maximum gradient increased with  $n$ . C and D: High contrast examples of two dark-to-light (DL) images, with exponents  $n = 1$  and  $n = 5$ . The reader may observe Mach bands in the right panel that are absent in the left panel.

$\sigma$ , while Figure 3B shows the corresponding second derivative profiles. Figure 3C reveals that the second derivative peak amplitude is almost directly proportional to the exponent  $n$  but falls as the inverse-square of scale  $\sigma$ ; hence the second derivatives at Scale 12 are 16 times lower than at Scale 3.

A sine-wave edge was also included in the test set. It was produced by integration of one half-cycle of a cosine function. The frequency of the cosine function (dashed curve in Figure 2A) was set to ensure that, like all the other gradient profiles, it fell to  $1/\sqrt{e}$  (61%) of its peak value ( $A_n$ ) at  $x = \pm\sigma$ . For the edge scales  $\sigma = 3, 6, 12$  min arc, the corresponding cosine half-periods were 10.25, 20.5, and 41 min arc.

### Experiment 1: Mach band detection

Image arrays were generated in Matlab on a Macintosh G4 computer and displayed using Psych-

Toolbox software on an Eizo 6600-M greyscale monitor, calibrated and gamma-corrected using a Minolta LS110 digital photometer. A Cambridge Research Systems Bits++ interface was used in Mono++ mode to render 14-bit greyscale resolution.

Images had one of two contrast polarities: dark-to-light (DL; Figure 2C and 2D) or a left-right reversal of this (LD). Image size was  $256 \times 256$  pixels and subtended  $4.26^\circ$  at a viewing distance of 123.4 cm. Test images had Michelson contrasts of 0.4 and were surrounded by a full-screen ( $16^\circ$  wide  $\times$   $12^\circ$  high) of uniform mean luminance ( $40.7 \text{ cd/m}^2$ ). At each of the three scales  $\sigma$ , there were 16 test images (eight waveforms, two polarities). Two examples are shown in Figure 2C and 2D.

A single-interval yes-no response method was used. Images were presented for 300 ms, preceded and followed by a mid-grey screen with a central fixation marker. Observers had unlimited time to press one of two buttons to indicate whether Mach bands had been

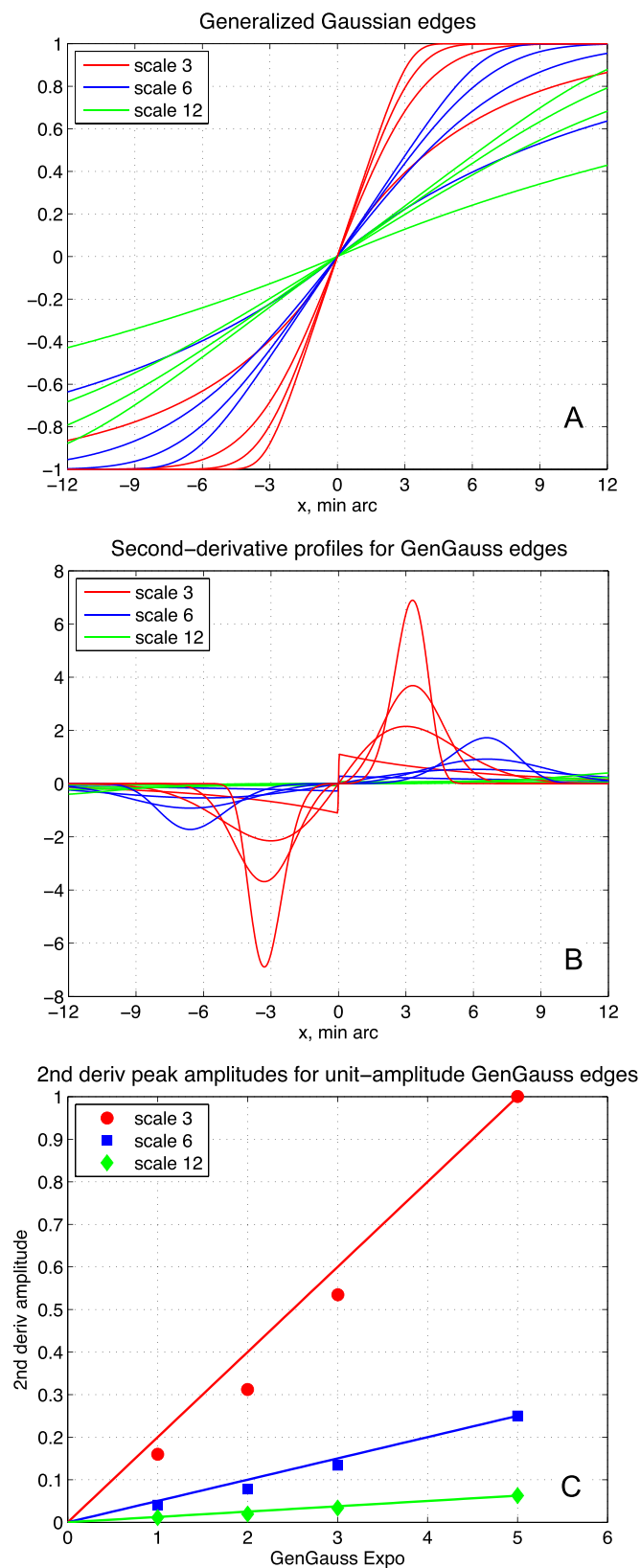


Figure 3. A: Luminance profiles for the family of generalized Gaussian edges used in the experiments. The form of each edge profile is defined by its scale (3, 6, or 12 min arc; red, blue, green curves) and its exponent  $n$ . At each scale, four examples are

perceived or not. Observers were instructed to report “yes” if they saw any Mach band, light, dark, or both. As in all yes-no experiments, the uncertain observer has to set their own criterion for saying yes or no. This criterion forms part of the model described later. A standard Mach ramp image—defined as a luminance ramp (of similar width to the  $n = 5$  waveform) flanked by two plateaux—was shown prior to data collection, as training. All 48 images (16 images at three scales) were shown five times in randomized order within one experimental session, which took about 10 minutes. Six observers completed seven sessions each, but the first session was discarded as practice. Only two observers (the authors) were aware of the stimulus design. All observers gave informed consent.

## Experiment 2: Feature-marking

Experiment 1 gave data about the probability of seeing Mach bands. In Experiment 2 these data were complemented by studying the geometry or spatial layout of Mach bands. We used a cursor to mark the position of each visible Mach band and the position of its edges.

The test images were the same as in Experiment 1 and were shown at the same contrast (0.4). Images were displayed flashing (on 300 ms, off 600 ms) in order to reduce the build-up of negative afterimages that cause instability and possible shifts in feature location (Georgeson & Turner, 1985). The interstimulus display was a full-screen of mid-grey.

A feature-marking method was used (Georgeson & Freeman, 1997) to identify the position and polarity of all edges and bars seen in each image. Their position was identified by the observer moving a marker across the image and pressing a button when the marker was over the center of an edge or bar. A second button-press indicated the identity and polarity of the feature as either a light-to-dark (LD) or dark-to-light (DL) edge or a light or dark bar. Observers were not forced to mark features they felt they could not see. Once all the perceived features had been marked, the observer initiated the next trial. The marker consisted of two black dots, each 1 pixel wide by 3 pixels high. One dot was centered 32 pixels (approx.  $0.5^\circ$ ) above the horizontal midline of the image, and the other was 32 pixels below the midline. The observer was instructed to fixate midway between the two dots. The starting

←  
shown:  $n = 1$  (shallowest), 2, 3, 5 (steepest). B: Second-derivatives of the waveforms shown in A, computed numerically. C: Peak amplitude of the second derivative (B), normalized to a maximum of one, varies nearly linearly with exponent  $n$  but as the inverse square of the stimulus scale ( $\sigma$ ).

position of the marker alternated between left and right on successive trials.

One session consisted of a randomized presentation of the image sets for all three image scales. Three observers (author SAW, DHB, NRH; all had taken part in Experiment 1) completed 10 sessions each, but the first session from each observer was discarded as practice.

### Experiment 3: Effects of contrast and duration on Mach band detection

The aim here was to examine how the probability of Mach band perception was affected by contrast and duration of presentation. The yes-no procedure of Experiment 1 was repeated for a single stimulus scale ( $\sigma = 6$  min arc) but with (a) three contrasts (0.2, 0.4, 0.8) at a presentation duration of 300 ms and (b) three presentation durations (50, 100, 300 ms) at a contrast of 0.4. There are only five different conditions here, and these five were presented in separate, randomly interleaved blocks of trials. The exponent  $n$  varied randomly from trial to trial ( $n = 1$  to 5) as before. There were five observers, including four who had taken part in Experiment 1. When pooled over the two polarities, there were 60 trials per condition per observer, as in Experiment 1.

## Results

### Experiment 1—Mach band detection

For each observer, the probability of reporting Mach bands was calculated from 60 trials for each condition and plotted against the generalized Gaussian exponent  $n$ . Observers' responses were similar for the two contrast polarities, and so group mean data, averaged across polarity, are shown in Figure 4. The probability of Mach band perception increased smoothly and monotonically as the generalized Gaussian exponent increased.

In a three-factor, repeated-measures analysis of variance, we confirmed that the effect of contrast polarity was not significant,  $F(1, 5) = 4.9$ ,  $p = 0.078$ , while the effect of exponent ( $n$ ) was highly significant,  $F(6, 30) = 107.6$ ,  $p < 0.0001$ . The main effect of spatial scale  $\sigma$  was not significant,  $F(2, 10) = 2.47$ ,  $p = 0.13$ , but the interaction between scale and exponent that is apparent in Figure 4 was statistically significant,  $F(12, 60) = 2.09$ ,  $p = 0.03$ . Selective analyses, with either Scale 3 or Scale 12 excluded, showed that this Scale  $\times$  Exponent interaction arose between Scales 3 and 6,  $F(6, 30) = 4.15$ ,  $p = 0.004$ , while there was no interaction

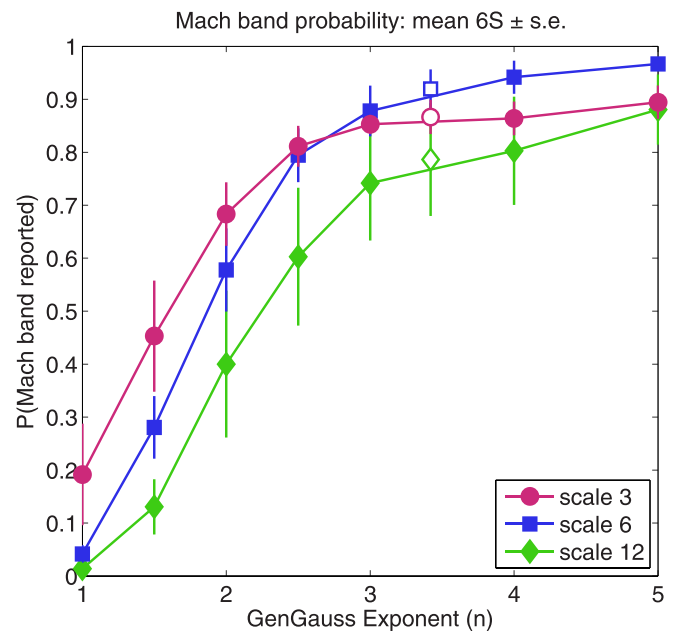


Figure 4. Experiment 1. Probability of seeing Mach bands on generalized Gaussian edges as a function of the exponent  $n$ . Mean of six observers  $\pm 1$  SE based on a total of 360 trials per point. Symbol shape and color denote image scale ( $\sigma$ ). Sine edge data (open symbols) have been inserted at  $n = 3.4$  (see text for details).

between Scales 6 and 12,  $F(6, 30) = 0.79$ , n.s. No other effects or interactions were significant. Thus to a large extent the occurrence of Mach bands was scale-invariant, but there was a tendency at the smaller exponents for the smallest-scale stimuli to give more Mach bands than the larger scales did, while Scale 6 gave the most Mach bands at the high exponents. The strong influence of  $n$  and the weak, nonsignificant influence of stimulus scale  $\sigma$  imply that the shape of the luminance waveform, rather than its size, is the key factor in Mach bands.

Mean data for the sine edge have been inserted on the exponent axis at  $n = 3.4$ . Figure 4 (open symbols) shows that this placement of the sine edge data provides a good fit with the rest of the data (and this was true also for individual observers—not shown). The value  $n = 3.4$  was obtained by fitting a smooth (Naka-Rushton) curve to each set of data points and then finding the point that minimized the total squared deviation between the sine-wave data and the curves. The fit was good ( $RMS$  error = 0.013). Put simply, this means that across the 18 datasets, the sine edge behaved most like a generalized Gaussian edge with an exponent of 3.4, as is evident in Figure 4. At all three scales, Mach bands were much more likely for sine edges (at  $n = 3.4$ ) than for Gaussian edges ( $n = 2$ ).

To assess their physical similarity, we computed the correlation between the luminance profiles of the sine

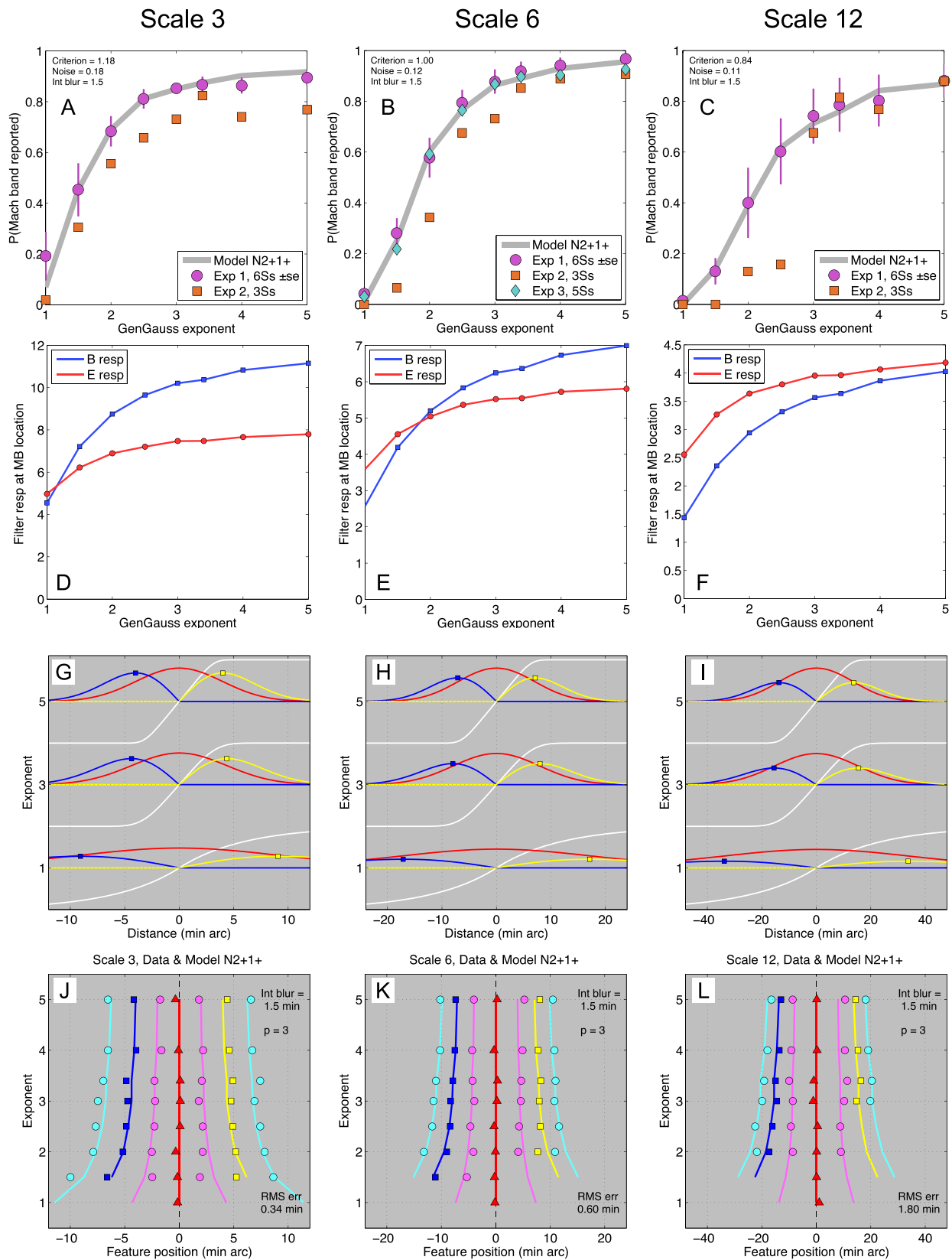


Figure 5. Data and model compared. A, B, C: Probability of reporting Mach bands, from Experiments 1 (circles), 2 (squares), and 3 (diamonds; averaged over three of the five conditions excluding the conditions at 50 ms and 0.2 contrast). Sine edge data plotted at exponent = 3.4. Grey curves show N2+1+ model's probability of reporting Mach bands, obtained with parameters shown in Table 1. D, E, F: Peak response of the Model B map (B<sup>+</sup> or B<sup>-</sup>, squares, blue curve) increased with exponent *n*. E response (red curve) at these B peak

→

edge and test edges with different values of  $n$ . This correlation was greatest (and the residual squared-error was least) when  $n = 3.2$ . The same was true for a comparison of their gradient profiles and also when each waveform was smoothed by a Gaussian whose blur  $b$  matched the edge scale  $\sigma$ . Our estimate of  $n = 3.4$ , based on similarity of Mach band probabilities, was thus close to the point of maximum physical similarity ( $n = 3.2$ ).

## Experiment 2: Feature-marking of Mach bands

Scatterplots were generated for each condition and observer and likely button-pressing errors were corrected by eye, e.g., where a single DL edge was marked within a spatial region of many LD responses. This was necessary for only 40 of the 23,988 responses. On each trial, the number of features marked ranged from one to seven, and grouping these responses in order to average them across trials is not trivial. Where seven were marked, they were taken to be derived from two Mach bands, their edges, and an additional edge near the image center. This assumption was supported by the typical pattern of responses, which consisted (for a dark-to-light image, marked from left to right) of LD edge, D bar, DL edge, DL edge, DL edge, L bar, and LD edge.

A Matlab program automatically parsed the data into seven feature bins according to logical rules. This was needed as responses in a single trial could contain up to three neighboring edges of the same polarity. The parsing rules are specified in [Appendix 1](#). The position of each Mach band was defined as the mean position within each bar bin.

The positions of Mach band features were similar across observers and image polarity, so average Mach band positions are shown for light and dark bands as yellow and blue squares, respectively, in [Figure 5J](#), [5K](#), and [5L](#). Points where a feature was marked on fewer than 10% of trials were omitted from the figure. For scales of 3, 6, and 12 min, the mean Mach band positions (taken over the range  $n = 2$  to 5) were 4.7, 8.0, and 14.7 min arc from the image center. Mach band position was therefore nearly proportional to the scale of the stimulus waveform.

The feature positions marked on stimulus waveforms of opposite polarity showed a small but systematic bias towards the side of the image that had lower luminance.

Helmholtz (2000, pp. 186–193) called this the “irradiation effect” (white squares look larger than black squares). We like to call it the *Darth Vader* effect—a shift to the dark side. The origin of this shift in edge positions may well be early compressive nonlinearity in the response to luminance (Mather & Morgan, 1986). Helmholtz noted that this explained why irradiation increases with optical blur—confirmed by Georgeson & Freeman (1997)—and we analyze it quantitatively later. For our data (Experiment 2) the bias was equally evident for edge and bar locations. To allow a better comparison between model and data, this small fixed bias was removed from the data by subtracting from each feature position the mean position of all the features marked for that stimulus scale at  $n \geq 2$ . For [Figure 5J](#), [5K](#), and [5L](#) this simply shifted the spatial origin to the mean marked position in each panel. For Scales 3, 6, and 12 these mean shifts to the dark side were 0.96, 1.25, and 2.12 min arc, respectively.

The width of a Mach band can be taken as the distance between the pair of opposite-polarity edges that flanked it (shown as pairs of cyan and magenta circles in [Figure 5J](#), [5K](#), and [5L](#)). Defined in this way, Mach band width increased markedly with the scale of the image. Mean width, again taken over the range  $n = 2$  to 5, was 5.1, 6.7, and 9.8 min arc at Scales 3, 6, and 12, respectively. Mach bands also became 20%–40% wider as exponent  $n$  decreased: At image scales 3, 6, and 12, mean widths were 1.16, 1.39, and 1.44 times wider, respectively, at  $n = 2$  than  $n = 5$ .

If Mach band perception were precisely scale-invariant then the patterns of features seen in the three scaled plots of [Figure 5J](#), [5K](#), and [5L](#) should all be identical (note that  $x$ -axis range is proportional to stimulus scale). Clearly they are similar, but at Scale 3 the bands were (relatively) wider and more separated than at Scales 6 and 12. We show below that a small degree of blur at the input can account for this departure from scale invariance.

## Experiment 3: Effects of contrast and duration

[Figure 6A](#) shows the mean proportion of Mach bands observed as a function of exponent  $n$  for the contrasts used here (0.2, 0.4, 0.8). Mach band probability increased with  $n$ ,  $F(6, 24) = 75.2$ ,  $p < 0.0001$ , as it did in Experiment 1, but showed only a

← positions also rose with  $n$ , but less steeply. B:E ratio therefore rose with  $n$ , and this produced the increasing response probability seen in A, B, C (grey curves). G, H, I: Examples of the response profiles (for  $n = 1, 3, 5$ , bottom to top in each panel) from which the B and E peaks were drawn in panels D, E, F. Luminance profile is white; E response is red; B<sup>-</sup> response is blue and B<sup>+</sup> response is yellow. J, K, L: Experiment 2. Comparison between full model (curves) and observed spatial layout (symbols) of Mach band features. Red triangles: central edge; blue, and yellow squares: dark & light Mach band positions; cyan and magenta circles: dark and light edges of Mach bands.

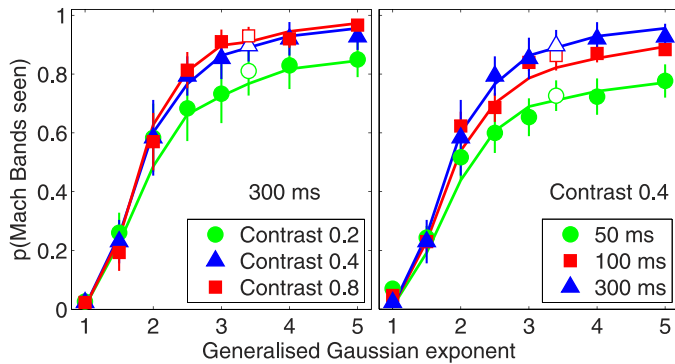


Figure 6. Experiment 3. Proportion of trials on which Mach bands were reported for generalized Gaussian edges of scale  $\sigma = 6$  min arc (filled symbols) and a sinewave edge (open symbols). Mean of five observers  $\pm 1$  SE. A: at three contrast levels (0.2, 0.4, 0.8) with duration 300 ms. B: for three durations (50, 100, 300 ms) at fixed contrast (0.4). Blue triangles (300 ms, contrast 0.4) are the same data in A and B. Curves show the fit of the multiscale model, as in Figure 5B, but allowing internal blur  $b_0$  to increase as contrast and duration decrease; see text for details.

small dependence on contrast in this suprathreshold range. Mach band probability was similar at contrasts 0.4 and 0.8, but a little weaker at lower contrast (0.2) for  $n > 2$ . The main effect of contrast was not significant,  $F(2, 8) = 1.63$ ,  $p = 0.255$ , but the interaction between contrast and exponent ( $n$ ) was significant,  $F(12, 48) = 2.9$ ,  $p = 0.0044$ . Such near-invariance with respect to contrast is important because the response of any linear filter increases in direct proportion to contrast, and so it follows that Mach band probability cannot depend directly on the response magnitude of linear filters. We consider below a model in which the perception of a bar, or Mach band, depends on the relative activation (the ratio) of even to odd filter responses, which is naturally contrast-invariant.

The effect of reducing duration (Figure 6B) was similar to that of reducing contrast. For  $n > 2$ , Mach bands were less visible at 50 ms than at 100 or 300 ms. This interaction between exponent and duration was highly significant,  $F(12, 48) = 3.17$ ,  $p = 0.002$ , though the main effect of duration was not,  $F(2, 8) = 3.42$ ,  $p = 0.085$ . We show below that the reduction in Mach band probability with brief or lower-contrast images can be explained by an increase in intrinsic blur.

The probability and geometry of Mach bands are approximately scale-invariant (Figures 4 and 5). We have seen (Figure 3B and 3C) that the amplitude of the second derivative of luminance is very far from scale-invariant and is therefore unlikely to be the controlling factor. We argue instead that it is necessary to compute the derivatives at multiple scales. Next we describe one such model (dubbed N2+1+), extending a multiscale edge-coding model (N1; Georgeson et al., 2007), but

now aiming to capture the location and scale of both bars and edges, using even- and odd-symmetric Gaussian-derivative filters in a scale-space framework.

## The N2+1+ model

The N2+1+ model, so-called because it uses scale-normalized second and first derivative operators in parallel, is sketched in Figure 1D. Examples of the scale-space response maps are discussed in Appendix 2. The basic model uses four parallel sets of channels—one for each edge polarity (dark-to-light or light-to-dark) and one for each bar polarity (light or dark). A third mechanism  $E_2$  (Figure 1D) is introduced to find the edges of Mach bands. All the filter kernels are spatial derivatives of the standard unit-area Gaussian function:

$$G(x, s) = \frac{1}{s\sqrt{2\pi}} \exp\left(\frac{-x^2}{2s^2}\right), \quad (2)$$

where  $s$  is the spatial scale.

## Edge response maps

The edge filters N1+ are as described in the N1 model of Georgeson et al. (2007), followed by half-wave rectification. The response map ( $E^+$ ) of the N1+ channel to an image  $I(x)$  is the convolution of the image with a Gaussian first-derivative filter

$$E^+(x, s) = \max\left[k_1 s^\alpha I(x) \otimes \frac{\partial}{\partial x} \left(G(x, s)\right), 0\right], \quad (3)$$

where  $s$  is the scale of the filter, ranging from 1 to 32 min arc in 0.02 octave steps,  $\alpha = 1/2$  is the scale normalization exponent (Lindeberg, 1998), and  $k_1$  is a constant that sets the relative strength of even and odd filter responses. The value of  $\alpha$  is chosen a priori to scale the filter response amplitudes, such that the peak response to a Gaussian edge of blur  $b$  occurs in the filter whose scale  $s = b$  (Georgeson et al., 2007). This means that the location of the peak response in scale-space encodes edge blur and position veridically, Figure A2(B). An expression for the scale-space edge map of opposite polarity ( $E^-$ ) is the same except that the  $\partial/\partial x$  filter is of opposite sign.

## Bar response maps

The response  $B^+$  of the light-bar channel (N2+) of scale  $s$  is defined by convolution with an even-symmetric Gaussian second derivative filter

$$B^+(x, s) = \max \left[ k_2 s^\beta I(x) \otimes \frac{-\partial}{\partial x^2} \left( G(x, s) \right), 0 \right], \quad (4)$$

where  $\beta$  is discussed below and  $k_2 = 1$  (fixed). The expression for the scale-space bar map of opposite polarity ( $B^-$ ) is the same as  $B^+$  except that the filter is of opposite sign. Mathematical analysis, confirmed by numerical computation, showed that choosing  $\beta = 3/2$  neatly achieves two things: the scale of the bar is veridically encoded (a bar of scale  $b$  produces peak response in the  $B$  filter that has scale  $s = b$ ), and the ratio of response amplitudes  $B/E$  is scale-invariant. If a signal is spatially magnified by some factor  $m$ , then the  $E$  and  $B$  response patterns are preserved: they are magnified by factor  $m$  and shifted in the (log) scale domain by factor  $m$ , while the  $E/B$  response ratio at  $(m.x, m.s)$  after the size change is the same as at  $(x, s)$  beforehand. A practical consequence of such scale invariance is that response ratios  $E/B$  would be independent of viewing distance. The experiments, however, suggest a slightly lower value for  $\beta$ , discussed below.

The model filter responses are half-wave rectified to create the  $B^+$  (light bar) and  $B^-$  (dark bar) responses, and these responses across many scales  $s$  can be visualized as scale-space response maps (Appendix 1). The image of a single light or dark bar produces a peak response at the center of the bar in one of the two maps ( $B^+$ ,  $B^-$ ), see Figure A1(A). The coordinates of this peak encode the position and scale of the bar. Its polarity is obtained from the identity of the map ( $B^+$  or  $B^-$ ).

Any bandpass spatial filter (including the Gaussian second derivative used here) produces more peaks and troughs in the response than there are luminance peaks and troughs in the image. For example the second derivative of a Gaussian bar is the familiar Mexican hat function—a peak flanked by two troughs. The same is true in the present model where  $B^+$  responses to a light bar are flanked by  $B^-$  responses, at all spatial scales, Figure A1(A). Some means is therefore needed for handling these multiple peaks to decide which ones represent visible features, and which do not. The MIRAGE model (Watt & Morgan, 1985), for example, used a set of parsing rules to classify features from filter responses. The N3+ model for edge detection (Georgeson et al., 2007) invokes third order Gaussian derivative filtering in two stages (first derivative followed by second derivative) and half-wave rectification at the output of each stage was designed to screen out spurious peaks and troughs introduced by filtering. For bar detection, however, no such strategy seemed viable, and instead we propose that a comparison between the four response maps may achieve similar ends (Figure A2). Notice how, in Figure A1(C) and A2(C), the peak responses for candidate bars (open squares) flanking a Gaussian edge or Gaussian bar,

might be screened out on the grounds that their response amplitudes ( $B^+$ ,  $B^-$ ) are lower than the edge responses ( $E^+$ ,  $E^-$ ) at the same scale-space point. Those candidate bars are occluded by the edge responses and so might be rejected as visible features. In a similar way, candidate edges (at peaks in the  $E^+$  or  $E^-$  maps) can be accepted or rejected by examining the edge:bar response ratios at those points. The present experiments support the view that such a comparative selection or decision process operates in human perception of Mach bands (see the section Noisy decision rule below).

## Intrinsic blur

A pragmatic factor required to fit the model to data was intrinsic blur. Blur in the display monitor and in the eye's optics are inevitable, but the amount of blur is not known precisely. In addition, high frequency attenuation due to nonoptical factors in the contrast sensitivity function may contribute a degree of effective blur that is not otherwise represented in our model. For simplicity, we bundled these three likely sources into a single Gaussian blur that was imposed at the model input (see Figure 1D), and we allowed the degree of blur to be a free parameter in fitting the data. For all the modeling shown in Figure 5, the intrinsic blur parameter ( $b_0$ ) was set to 1.5 min arc—small enough to suggest that display blur and dioptric blur (at the eye) were the main sources. We also show (below) that this intrinsic blur increases at lower contrast and short duration (Figure 6). For a further discussion and critique of the concept of intrinsic blur, see Watson and Ahumada (2011).

## Mach band geometry: Fitting the model

The model has many spatial filters, but these are highly constrained with few free parameters, summarized in Table 1. Here we describe how the parameter values were selected on the basis of theory and data. The model was first used to estimate the positions of Mach bands across the whole stimulus set. Importantly, these predictions about the geometry of Mach bands depend only on the image filtering stages of the model and are independent of assumptions about the noisy decision process described below. Thus the fit to about 150 data points (Figure 5J, 5K, and 5L) was achieved with just five parameters (top half of Table 1), only three of which were adjusted to fit the data. The factors controlling Mach band position were the  $B$  scaling exponent  $\beta$  and the input blur  $b_0$ . The assumption of scale invariance of the  $B:E$  ratio led us to expect a theoretical value of  $\beta = 1.5$  (see above) but the data did

Filtering scheme	Source		
Intrinsic blur	$b_0$	1.5 min	Band position data; fitted
E scaling exponent	$\alpha$	0.5	Theory; fixed
B scaling exponent	$\beta$	1.15	Band position data; fitted
$E_2$ nonlinearity	$\rho$	3	Edge position data; fitted
$E_2$ scale	$s_0$	1.5 min	Fixed = $b_0$
Filter comparison and noisy decision			
E gain	$k_1$	0.37	Band probability data; fitted
B gain	$k_2$	1	Fixed
$E_2$ gain	$k_3$	1.6	Not used to fit data
Criterion, scale 3	$c$	1.18	Band probability data; fitted
Criterion, scale 6	$c$	1	Fixed
Criterion, scale 12	$c$	0.84	Band probability data; fitted
Noise, scale 3	$v$	0.18	Band probability data; fitted
Noise, scale 6	$v$	0.12	Band probability data; fitted
Noise, scale 12	$v$	0.11	Band probability data; fitted

Table 1. Parameters for the N2+1+ model.

not support this. The peak filter scales were too large and in consequence the predicted bands were too far apart. A much better fit was obtained with  $\beta = 1.15$ . The choice of blur  $b_0 = 1.5$  min arc was largely dictated by Mach band positions at Scale 3 (Figure 5J); smaller values of  $b_0$  led the predicted light and dark bands to lie markedly closer together than the observed ones. With these choices for  $\beta$  and  $b_0$ , dictated by the data, the model's Mach band positions are shown as blue and yellow lines in Figure 5J, 5K, and 5L. These are close to the mean marked positions (blue and yellow squares). Both the model and observed positions varied little with exponent  $n$ , but the model does seem to correctly capture a small increase in Mach band separation at low exponents ( $n < 3$ ).

### Noisy decision rule and its application to Mach band probability

The N2+1+ model returns the location and scale of bar features, but in the absence of noise the probability of report is one or zero. To explain why different stimuli evoke systematically different probabilities of Mach band perception, we used standard signal detection theory to add a noisy decision process to the noise-free signal processing considered so far.

On each trial, the observer is assumed to base his or her Mach band decision (yes or no) on the ratio of the outputs of the B and E channels. These ratios are obtained from the scale-space maps at the peaks in the bar maps ( $B^+$  or  $B^-$ ). If the B:E response ratio is above some criterion  $c$ , the observer says “yes”; otherwise “no”. This response ratio is assumed to vary because of added Gaussian noise. Thus the B:E ratio is Gaussian-distributed with mean  $r$  and standard deviation  $v$ . The

probability of a yes is the area under this distribution that lies above the criterion, and the probability  $p$  of a yes is obtained from its  $z$ -score

$$p = \Phi\left(\frac{r - c}{v}\right), \quad (5)$$

where  $\Phi(z)$  is the standard normal integral. Six parameters were adjusted (see lower half of Table 1; equivalent to two free parameters per stimulus scale) to obtain a good fit by eye between model and observed Mach band probabilities across all three scales (thick grey curves in Figure 5A, 5B, and 5C). Although the parameters were selected to fit the data, it is not trivial that excellent fits were obtained. If the B:E ratio did not rise monotonically with exponent  $n$ , no good fit would be possible.

In summary, the model inputs were first slightly blurred, then spatially filtered at multiple scales by even (Gaussian second derivative, N2+) and odd (Gaussian first derivative, N1+) filters, and then bar features (Mach bands) were found (or rejected) at peaks in the  $B^+$  or  $B^-$  scale-space response maps by a noisy comparison of B:E responses at those peak points.

To visualize the steps in this process, consider the middle column of Figure 5 (stimulus scale 6 min arc). For stimulus exponents  $n = 1, 3$ , and 5, the yellow and blue curves in Figure 5H show the spatial profiles of responses  $B^+$ ,  $B^-$  at the optimal filter scale; each is a cross-section through the scale-space map. Blue and yellow squares mark the peak B responses, and the probability of a Mach band response depends on the height of that point relative to the edge response (red curve) at the same scale-space point. Moving up to Figure 5E, we see that both the B and E responses at these peak points increase with exponent  $n$  but the bar response (B) rises more steeply and so the B/E ratio ( $r$  in Equation 5) rises with  $n$ . This in turn makes the model's Mach band probability increase with  $n$  (thick grey curve, Figure 5B).

Symbols in Figure 5B show the observed probabilities from Experiments 1, 2, and 3. There is very good agreement across the three experiments (even though Experiment 2 had far fewer trials and was not designed to estimate the probability). With suitable choice of criterion and noise level in the model (values  $c$  and  $v$  in Table 1), the model and observed probabilities are in good agreement. Model fits for Scales 3 and 12 are presented in the same way in the left and right columns of Figure 5.

In short, with reasonable assumptions about the decision criterion ratio ( $c = 0.8$  to 1.2) and internal noise ( $v$ ), the probability of reporting Mach bands can be well described from the way the bar:edge (B/E) response ratio varies with the exponent  $n$ . At all three scales the B/E ratio is low ( $r < 1$ ) when  $n$  is low ( $n < 2$ ) and rises monotonically with increasing  $n$ . Mach bands

are more probable on Mach ramps (with sharp corners; high  $n$ ) because the B/E ratio is well above the criterion ( $r > c$ ), but for Gaussian-like edges ( $n \approx 2$ ) the bar:edge response ratio is about equal to the decision criterion (giving  $z \approx 0$ ), hence the probability of reporting Mach bands is only about 50%. Despite the apparent similarity in their waveforms, the probability of seeing bands on a sine edge was markedly higher than on a Gaussian edge, and this difference is well captured by the model.

## Influence of contrast on Mach bands

In our model Mach bands arise from peaks in the response of even-symmetric, second derivative filters but, as anticipated in the [Introduction](#), Mach band strength does not depend directly on second derivative amplitude, neither at a single scale nor at multiple scales. Instead we have proposed that it depends on the ratio of even-to-odd filter responses. For linear filters, this ratio is invariant with contrast and so predicts that Mach band probability should also be contrast-invariant. This rather surprising outcome was confirmed in part by Experiment 3 where doubling the contrast from 0.4 to 0.8 did not increase the probability of Mach band reports. But at a lower contrast (0.2) the probability of Mach bands was lower ([Figure 6A](#)). We suggest that this reduction comes from a relative loss of visibility of the higher spatial frequencies that are critical to the visibility of the bands (Ross et al., 1989). We found that the reduction in Mach band probability at lower contrast and shorter duration can be rather precisely described by our model with increases in intrinsic blur  $b_0$ . Curves in [Figure 6](#) show the fit of the model, computed exactly as for [Figure 5](#), but allowing intrinsic blur to increase at lower contrasts and briefer durations. In [Figure 6A](#), intrinsic blurs  $b_0 = 3, 1.5, 1$  min arc gave excellent fits at contrasts 0.2, 0.4, 0.8, respectively. Similarly, in Panel B, blurs  $b_0 = 3.5, 2.5, 1.5$  min arc accounted well for the data at 50, 100, 300 ms.

Why should reducing contrast or duration increase intrinsic blur? At low contrasts, spatial vision is compromised by noise and uncertainty, and we can expect perception of the higher spatial frequencies to become relatively attenuated and eventually undetectable at contrasts for which the lower frequencies remain visible (Campbell & Robson, 1968; Georgeson & Sullivan, 1975). Thus reduction of contrast may produce effects that are equivalent to an increase in blur, as we saw in [Figure 6A](#). The visibility of Mach bands was closely associated with the visibility of the higher spatial frequencies (Ross et al., 1989), and Mach bands were not seen at all for ramps whose contrasts were less than about 0.1 (Ross, Holt, & Johnstone,

1981; Ross et al., 1989). Thus our test contrast of 0.2—fairly close to the Mach band threshold—may have suffered this effective blurring while contrasts of 0.4 or 0.8 did not.

A similar argument can be invoked for short durations. For example, when compared with long presentations (160 ms), contrast thresholds at short duration (40 ms) were raised by a similar factor at low and high spatial frequencies (Georgeson, 1987; Legge, 1978) and this might suggest no effective increase in intrinsic blur. But if instead we consider perceived contrasts above threshold, it was found that short durations reduced the perceived contrast of high spatial frequencies but did not reduce, and sometimes enhanced, the perception of lower spatial frequencies (the classic Broca-Sulzer effect) (Georgeson, 1987). This implies that broadband images should suffer an effective blurring at brief durations, consistent with our modeling in [Figure 6B](#).

## Problem: The edges of Mach bands

The positions of peak responses in the bar maps  $B^+$  and  $B^-$  correspond very well with the observed locations of Mach bands (squares in [Figure 5J, 5K, and 5L](#)). This depended on an appropriate choice for the scaling exponent  $\beta$  ([Equation 4](#)). Nevertheless, despite this success, there remains a substantial problem—the edges of Mach bands. Our observers marked the bands as having edges, with the systematic layout seen in [Figure 5J, 5K, and 5L](#).

As far as we know, the only previous work to recognize that Mach bands have edges and that these are a problem in need of explanation is the unpublished report of Ludvigh (1953a). As in our experiments, his observers used a pointer to mark the perceived edges on waveforms that appear (from our analysis of his [Figure 5](#)) to be very similar to the sine edges we used. We extracted and replotted his data and found that the perceived position of the bands (taken as the mean position for each pair of marked edges) and the width of the bands (the separation between the edges) were similar to ours and increased with edge scale in a similar way. Ludvigh was keen to promote the role of higher spatial derivatives in vision and was struck by the fact that edges could be seen at image locations where the gradient (first derivative) was close to zero: “If the significance of the higher derivatives for the formation of contours is as great as it appears to be, then we have found which feature of the physical world chiefly carries visual ‘intelligence’” (Ludvigh, 1953a, p. 9). We have much sympathy with this view, and yet it seems to us that Ludvigh (1953a, 1953b) did not actually propose a theory for these edges.

There must necessarily be some neural process that enables the edges of Mach bands to be found, but neither the N1+ model examined here nor the N3+ model (Georgeson et al., 2007) that we also explored extensively predicts any edges for Mach bands in our experiments. We strongly suspect that no other standard model of edge-detection would find these edges either. The test images contain luminance gradients of only one sign, and this means that for a given test image the N1+ and N3+ models can at best predict edges of only one polarity, because by design each edge channel is gradient-polarity-specific. We found that the N1+ model yields only a single central edge—and no edges for the Mach bands—because its scale-space response has just a single central peak, for any  $n$ . The N3+ model can produce one of the two edges for each Mach band (the inner edge, closer to the center of the image), but only when the corner in the luminance profile is sufficiently sharp, e.g.,  $n = 10$ , outside the range of our experiments.

The N3+ model does correctly predict the Mach edges that are seen flanking the peaks and troughs of blurred triangle wave gratings (Wallis & Georgeson, 2009). For these stimuli the *gradient profile* (rather than the luminance profile) is a Mach ramp, and so the Mach edges are the analog of Mach bands but shifted up by one derivative order; they emerge as peaks in the third derivative rather than the second. But we now see that the edges of Mach bands are a different problem that requires a new solution, as follows.

## Solution: A second route to edges, $E_2$

We propose that the output of the  $B$  mechanisms implicitly contains information about the edges of bars and Mach bands, and that the  $B$  output is further processed via an accelerating nonlinearity to make them explicit. Our underlying philosophy is the same throughout: that simple, feed-forward, signal processing—combining (a) multiscale linear Gaussian derivative filtering, (b) pointwise nonlinearities (half-wave rectification, power function transduction), and (c) peak-finding in scale-space—should suffice to locate and identify features, without logical parsing rules or top-down intervention. For example, colored curves in Figure 7B show how peaks in the gradient of the (linear)  $B$  response (black curve) do not capture the edges of Mach bands. There are four edges to be explained but only three extrema in this smoothed third derivative. On the other hand, raising the magnitude of the  $B$  response to some power  $p > 1$  (here,  $p = 3$ ) while preserving the sign sharpens and squeezes the  $B$  response (black curve in Figure 7C). It then has four (rather than three) points of steepest gradient, and so taking its derivative does lead to four extrema (colored

curves, Figure 7C) that correspond well with the observed edge positions (circles).

Figure 7D illustrates a simple variant of that idea in which, consistent with our general approach, only positive outputs are used and sign or polarity is carried by parallel channels. To find the edges of Mach bands the proposed chain of operations  $E_2$  is a form of nonlinear third derivative (analogous to, but different from, N3+). As shown in Figure 1D, we take the second derivative map  $B^+$  or  $B^-$ , pass its (always-positive) values through an accelerating transducer (with power  $p$ ), filter again with a gradient (Gaussian derivative) operator, half-wave rectify, take the  $p$ th root, then find peaks in scale-space as usual using the  $E_2/B$  ratio to decide how probable those edges are, via Equation 5. Note that the power  $p$  operation is crucial, but the  $p$ th root is not so critical, because it does not alter the peak locations introduced by the previous steps. Taking the  $p$ th root does, however, render the response linear with respect to contrast, and so makes the  $E_2/B$  ratio contrast-invariant.

The  $E_2$  response maps are defined by expressions of the form

$$E_2^+ \{B^+(x, s)\} = k_3 \left\{ \max \left[ B^+(x, s)^p \otimes \frac{\partial}{\partial x} (G(x, s_0)), 0 \right] \right\}^{\frac{1}{p}}, \quad (6)$$

where  $p = 3$ ,  $k_3$  is a constant, and  $s_0$  is a small fixed scale that was set equal to the intrinsic blur value ( $s_0 = b_0 = 1.5$  min arc). The  $E_2$  map needs to come in four flavors to capture the positive and negative edges of light bars and dark bars, respectively. These four variants are obtained by using either the  $B^+$  or  $B^-$  map as input, combined with a positive or negative sign on the  $\partial/\partial x$  filter. Thus a peak in the map of Equation 6 represents the left-hand (light) edge of a light bar. Its right-hand (dark) edge would be captured by peaks in

$$E_2^- \{B^+(x, s)\} = k_3 \left\{ \max \left[ B^+(x, s)^p \otimes \frac{-\partial}{\partial x} (G(x, s_0)), 0 \right] \right\}^{\frac{1}{p}}, \quad (7)$$

while the light and dark edges of a dark bar would be found using  $B^-$  rather than  $B^+$  as the input map. An interesting consequence of this four-channel scheme (Figure 7D) is that the system not only finds the light and dark edges of Mach bands, but it also knows (from the identity of the channel) what the polarity is and whether those edges arose from, or belong to, a light bar or a dark bar.

Finally, Figure 8 illustrates the full model's scale-space response maps (a composite of the eight maps for

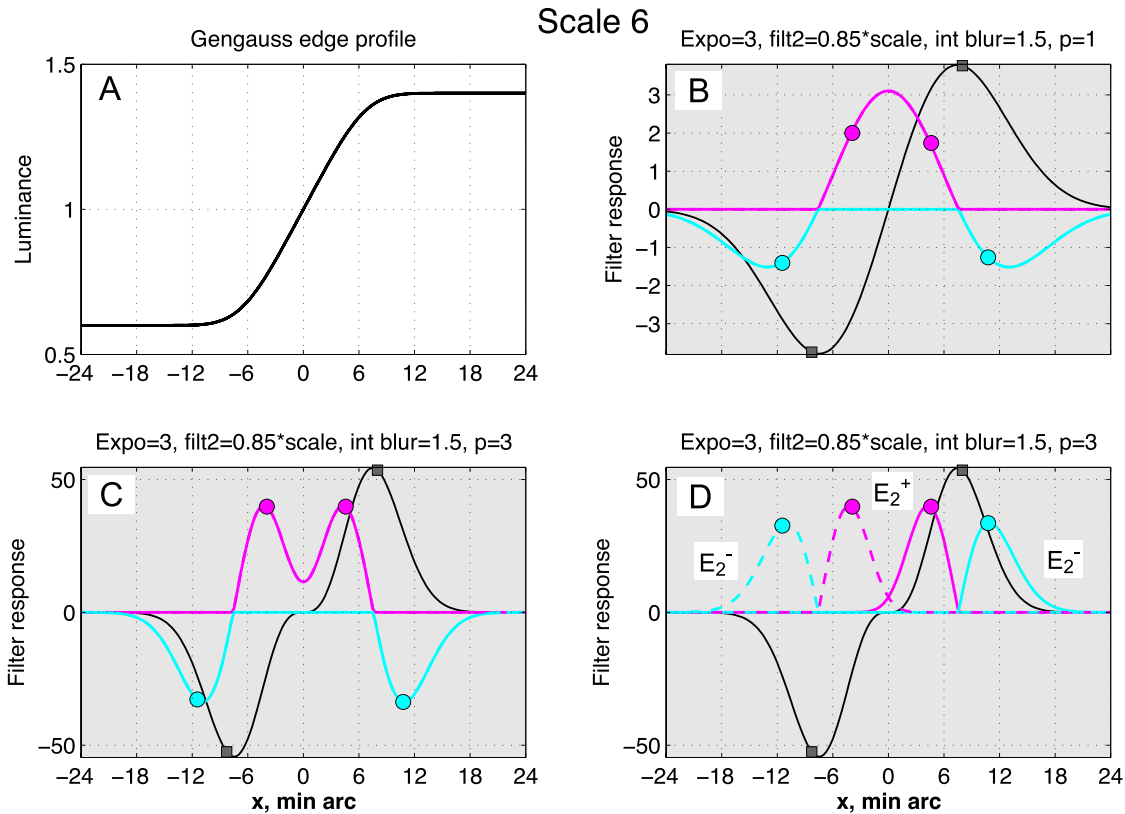


Figure 7. Finding the edges of Mach bands: problem and solution. A: Luminance profile of an edge with  $n=3$ ,  $\sigma=6$ . B: black curve shows the corresponding output of a Gaussian second-derivative filter. Black squares show that peaks are in good agreement with positions of Mach bands observed in Experiment 2 (seen more fully in Figure 5). Vertical position of these data is arbitrary, so they are simply placed on the model curve to which they relate. Colored curves show positive and negative parts of the gradient of the black curve (Gaussian derivative, computed with fixed scale  $s_0 = 1.5$  min arc). Problem: The perceived edges of Mach bands (circles) don't correspond with peaks, troughs, or zero-crossings in either of these derivatives. C: Solution: As B, but the magnitude of the second-derivative filter output (black curve in B) has been raised to power  $p$  ( $p=3$ ) with preservation of the sign before the third derivative operation. Peak position and sign now correspond well with the perceived edges of Mach bands. D: A simple variant of the scheme in Panel C, in which, via half-wave rectification, different channels are used to carry features of opposite polarity. Colored solid curves represent the positive and negative parts of the derivative of  $(B^+)^p$  while dashed curves show the same for  $(B^-)^p$ . Peaks in these four sign-specific  $E_2$  channels correspond well with the perceived edges of Mach bands (filled circles). Note: These worked examples used a single scale ( $s = 0.85 \cdot \sigma = 5.1$  min arc) for the B filter, but the full multiscale model was used for Figure 5, as illustrated in Figure 8.

$E^{\pm}$ ,  $B^{\pm}$ , and  $E_2^{\pm}\{B^{\pm}\}$ ), along with the features found in those maps, for test images with exponents  $n = 1, 2, 3$ , and 5 and scale 6 min arc. The maps for exponents  $n = 2, 3$ , and 5 (Figure 8B, 8C, and 8D) show Mach bands (blue and yellow squares), but the bands are weak (open symbols) in the map for  $n = 1$  (Figure 8A). All four maps show the central DL edge (red triangle) that is seen in the data of Figure 5J, 5K, and 5L. The edges of Mach bands (circles) emerge more reliably as  $n$  increases.

With the addition of the  $E_2$  mechanism, we can now see in Figure 5J, 5K, and 5L how well the full model (Figure 1D, Figure 8) is able to account for the positions of Mach bands (blue and yellow curves) and their edges (cyan and magenta curves). The goodness-of-fit is clear and the RMS errors are strikingly low, with little or no systematic residual error. The gradual divergence of

band and edge positions as  $n$  decreases is well described, especially for the dark bands (left side of each panel).

The predicted separation between the two edges of a Mach band is controlled by the power  $p$ . Raising the power  $p$  squeezes the B response profile (Figure 7) even more and so decreases the separation between the edges. For simplicity we set  $p$  to a single value ( $p = 3$ ) and this gave an excellent fit for all three stimulus scales. This proposed nonlinearity is consistent with earlier findings. The value  $p = 2$  represents half-squaring of the linear filter output—a common property of physiological models for V1 cells (e.g., Heeger, 1992)—but higher values of  $p$  are common in the physiological and psychophysical literature. Values of  $p$  between two and three are typically used to model the response nonlinearity at low contrasts in contrast

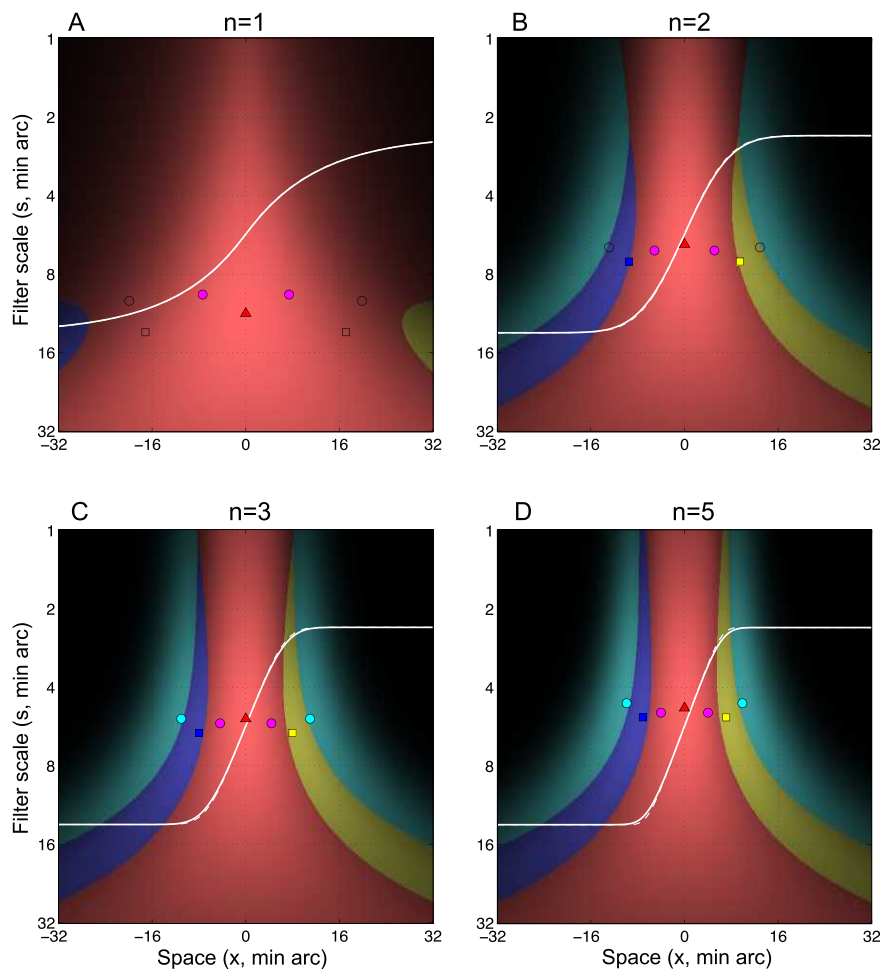


Figure 8. Scale space map and features found by the full N2+1+ model for test images ( $\sigma = 6$  min arc) with exponents  $n = 1$  to 5. The map is a color-coded composite, representing the max at each point over the eight contributing maps. Blue and yellow regions are (part of) the bar response maps ( $B^-$  and  $B^+$ ); pink region is from the edge response map ( $E^+$ ); cyan regions are from the two  $E_2^-$  maps; magenta regions (the  $E_2^+$  maps) are entirely hidden behind the  $E^+$  map. A, B, C, and D: As  $n$  increases, the corners in the luminance profile (white curve) sharpen; Mach bands emerge (blue and yellow squares) and shift progressively towards smaller scales. Open squares for  $n = 1$  show potential Mach bands in the bar maps that are occluded by a higher response in the edge map. Red triangle is the very salient central edge from the  $E^+$  map, while cyan and magenta circles are the edges of Mach bands from the  $E_2$  maps. Solid white curve is the luminance profile after blurring ( $b_0 = 1.5$  min arc); dashed curve, where visible, is the luminance profile before blurring.

discrimination experiments (Foley & Legge, 1981; Legge & Foley, 1980; Nachmias & Sansbury, 1974).

### Single-scale models

There is a wealth of evidence that the early visual system filters and encodes data at multiple spatial scales, and our scale-space peak-finding model is evidently successful in its application to the perception of edges and Mach bands. But it is reasonable to ask whether, or to what extent, a simpler single-scale model might suffice. We addressed that question by forcing the model to use just a single filter scale, then computing the *RMS* error between predicted and observed feature locations for Experiment 2, just as in Figure 5, with all

parameters unchanged. The goodness-of-fit, assessed by *RMS* error, is plotted in Figure 9 as a function of the filter scale used. For each stimulus scale ( $\sigma$ ) there was a clear point of minimum error, implying an optimum filter scale, and this optimum increased roughly in proportion to the scale of the stimulus.

Perhaps surprisingly, the best goodness-of-fit in the single-scale cases was as good as, or a little better than, the fit of the multiscale model (marked by three horizontal lines in Figure 9). Does this mean that the multiscale nature of our model is unnecessary? We think not. To find the optimum single scale (at the minima in Figure 9) we had to test many filter scales for each stimulus scale, then choose the best one in each case using prior knowledge of the perceived features' identity and location (the experimental data). But, like

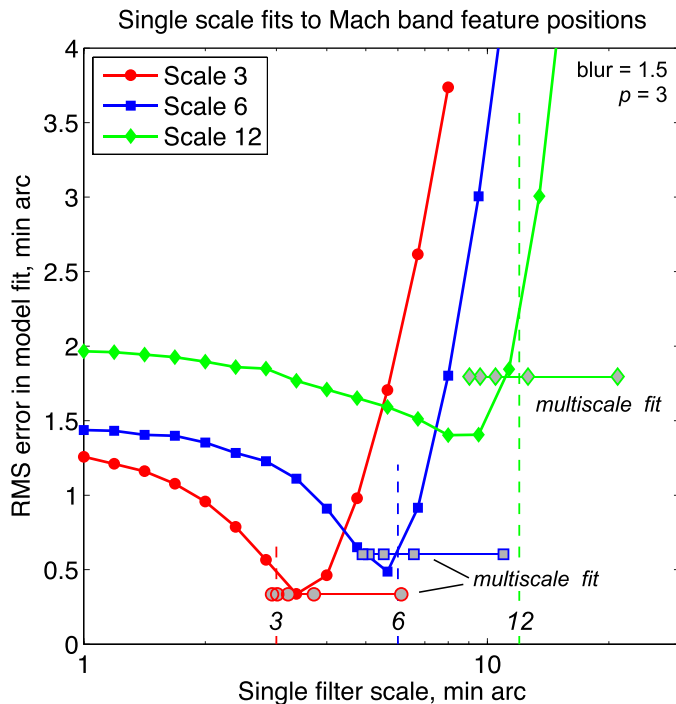


Figure 9. Goodness-of-fit for single-scale models. The full model (Figure 5) was constrained to use a single fixed scale for the E and B filters, and the *RMS* error in predicted feature positions (taken over exponents  $n = 2$  to 5;  $N = 42$  data points) is plotted against the filter scale used, for edge Scales 3 (red curve), 6 (blue curve), 12 (green curve). For comparison, horizontal lines mark the corresponding goodness-of-fit for the multiscale model, from Figure 5. The five points on each line indicate, reading from right to left, the average filter scale selected by the multiscale model for each of five exponents ( $n = 1, 2, 3, 4,$  and  $5$ ), averaged (geometric mean) over the seven features found for each stimulus.

the real visual system, the multiscale model did not enjoy this luxury of extrasensory perception, and its automatic selection of filter scales was driven entirely by the stimulus input interacting with the structure of the filtering system. That is a key insight drawn from Lindeberg's (1998) analyses of Gaussian-derivative scale-space, implemented here by suitable choice of scaling exponents  $\alpha$  and  $\beta$ .

Nevertheless, it was surprising that a single filter scale—albeit hand-picked—could work so well (Figure 9). We think this occurs because, with this stimulus set, even the multiscale model picks a very limited range of filters for a given stimulus and so a single filter scale—chosen for that stimulus—can produce a similar outcome. A glance at Figure 8 confirms that for a given exponent (e.g.,  $n = 3$ , Figure 8C), nearly the same filter scale is picked for all seven features. These filter scales shift to smaller values as exponent  $n$  increases (Figure 8D). This is quantified in Figure 9 by the leftward progression of the five grey-filled points that represent the geometric mean filter scale for each of the exponents

$n = 1$  to 5. For  $n = 1$  the filter scales were about an octave higher than the rest, but for  $n = 2$  to 5 (the four leftmost points on each horizontal track), the mean scales clustered quite closely together and the mean of this cluster was, in all three cases, close to the optimum single scale. In short then, in the range  $n \geq 2$  for which the *RMS* error was computed, the mean filter scale selected by the multiscale model was close to the best single scale. This explains why a fixed scale can substitute for variable scale selection. Importantly, both analyses tell us that to account accurately for the layout of the bar and edge features, the filter scale must increase with the stimulus scale: visual filtering is multiscale.

There was no single filter scale that was optimum over all three stimulus scales, and we emphasize that to select a single scale requires unrealistic prior knowledge of the stimulus. The multiscale model therefore has several important advantages over its single-scale counterparts. The functional advantage of automatic, localized scale selection would be much more apparent for images that (unlike our test images) contained a wider range of sharp and blurred features in different locations.

## Nonlinear response to luminance: The shift to the dark side

We noted earlier that the marked features (Experiment 2) exhibited a systematic shift to the dark side of the edge, and to keep the model simpler we removed that small (1–2 min arc) effect from the data by subtracting the overall mean position. Having developed a successful model, we can now return to the uncorrected data to ask whether, with nonlinear transduction of luminance (a model photoreceptor), the same model can predict this shift to the dark side while preserving the correct pattern of observed features.

The model transducer was a standard Naka-Rushon function

$$I(x) = (1 + S) \frac{L(x)}{S.L_0 + L(x)}, \quad (8)$$

where  $L(x)$  is the input luminance profile (after blurring by the display and the eye; Figure 1D),  $L_0$  is the mean luminance,  $S$  is the semisaturation constant, and  $S.L_0$  is the semisaturation luminance. The constant term  $(1 + S)$  is a convenient normalizing factor that implies  $I = 1$  when  $L = L_0$ . Note that  $S$  is expressed in units of  $L_0$ , and so a given value of  $S$  represents a certain degree of compressiveness in transduction independently of mean luminance. Lower values of  $S$  produce a more compressive response to luminance while higher values tend towards linearity. Georgeson & Freeman (1997) measured and modeled the perceived offset of blurred

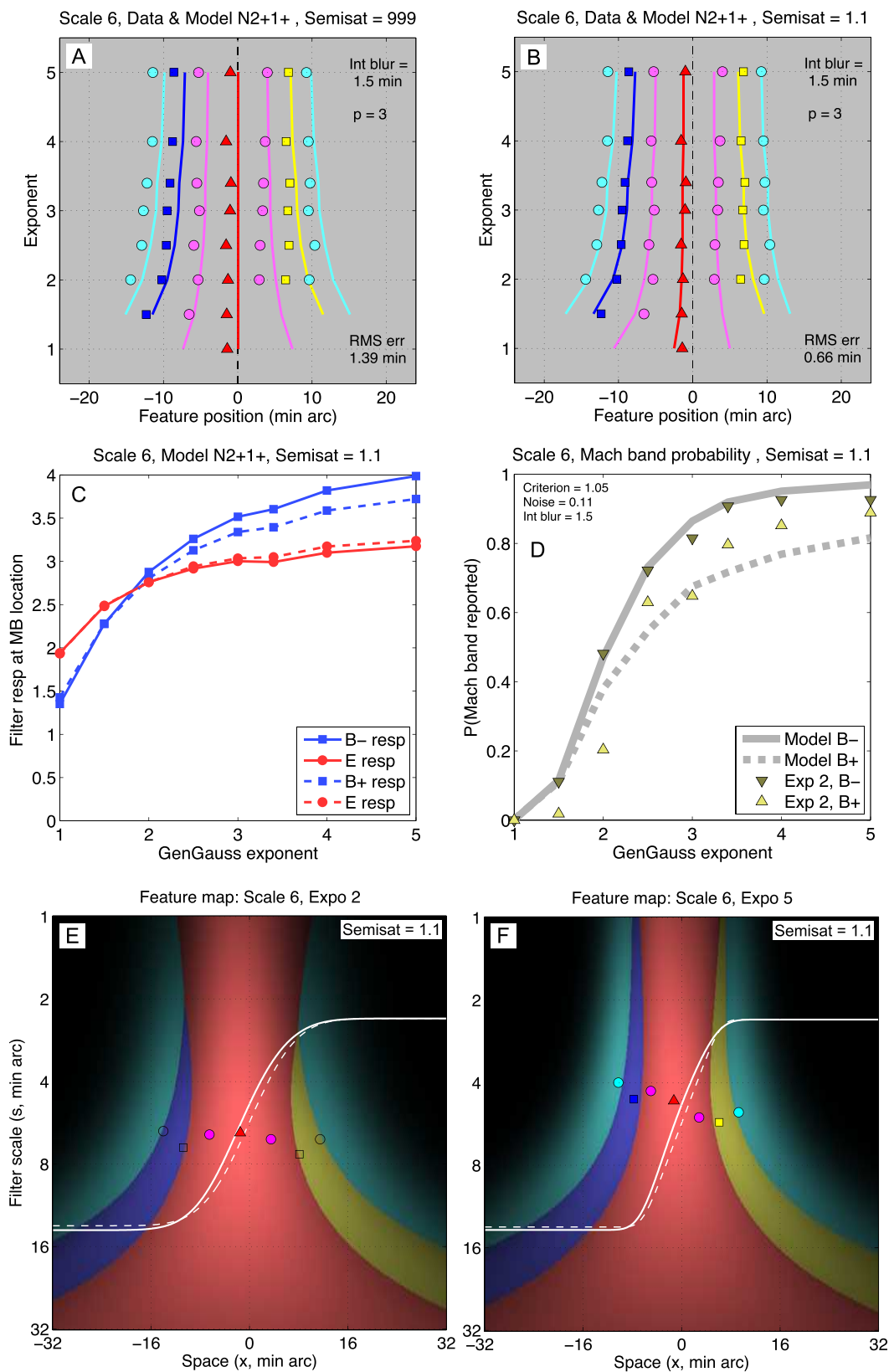


Figure 10. Nonlinear response to luminance explains why features shift to the dark side. A: Linear response to luminance. Curves: model feature positions (Scale 6, dark to light stimulus edge); symbols: experimental data with no correction for the shift to the dark side. Offset of data to the left of the model is obvious. B: Model with a nonlinear response to luminance captures this offset very well. C: E and B filter responses plotted separately for the dark band (B<sup>-</sup>, solid curves) and the light band (B<sup>+</sup>, dashed curves). D: Predicted probability of dark

→

edges towards their darker side and concluded that a value of  $S$  between 0.5 and one was broadly consistent with the observed magnitudes of the offset. Here we chose  $S = 1.1$  to model the data of Experiment 2 and used  $S = 999$  to represent the linear response.

With linear transduction the model, as expected, showed no shift of feature positions to the dark side; curves in Figure 10A (same as in Figure 5K), are symmetrical about  $x=0$ . In contrast, symbols in Figure 10A show experimental data from Experiment 2 now plotted with no correction. Systematic offset of data to the left (the darker side) is obvious, and *RMS* error in model fitting (1.39 min arc) was more than doubled compared with Figure 5K. But with the inclusion of a nonlinear response to luminance ( $S = 1.1$ ), the model captured both this offset and the pattern of feature positions very well indeed (Figure 10B). *RMS* error was low (0.66 min arc) and almost as good as for the hand-crafted correction (0.60 min arc; Figure 5K). This analysis has considered Scale 6, but similar results were obtained at Scales 3 and 12. Averaged over  $N = 42$  features ( $n \geq 2$ ) the model predicted mean dark shifts of  $-0.62, -1.06, -2.02$  min arc for stimulus Scales 3, 6, 12, and this agreed well with the observed mean shifts of  $-0.96, -1.25, -2.12$  min arc, respectively.

Our finding that Mach bands, as well as edges, are shifted a little to the darker side is not trivial. Bars or lines that arise from a physical, symmetrical, luminance peak cannot be shifted laterally by compressive transduction, because symmetry is preserved. But the Mach band stimulus is not symmetrical, and there is no luminance peak. Compressive transduction modifies the luminance profile (Figure 10E and 10F), and this in turn alters the first and second derivatives. Peaks in both these derivatives shift to the darker side as Figure 10B has shown.

The compressive response to luminance predicts a second, rather subtle effect: The dark bands should be a bit more visible than the light bands. Figure 10C shows why: The E and B filter responses are plotted separately for the dark band ( $B^-$ , solid curves) and the light band ( $B^+$ , dashed curves). The compressive luminance response smooths the upper corner of the luminance profile (see Panels E and F), reduces the  $B^+$  response and the  $B^+/E$  ratio, and so leads to fewer “yes” responses for the light band than the dark band. These predictions (Figure 10D, solid and dashed grey curves) gain some support from the data of Experiment 2, showing that observers marked fewer light Mach bands (light triangles) than dark Mach bands (dark triangles).

Such a difference was also evident in the data for Scale 12, but not at Scale 3. A yes-no experiment with more statistical power, many more trials, and independent judgments of light and dark bands would be needed to confirm this finding. Further support comes from earlier findings that increment thresholds (Thomas, 1965) and contrast thresholds (Ross et al., 1989) for seeing the dark bands were systematically lower than for the light bands, implying greater visual sensitivity for the dark bands. Ross et al. (1989) suggested that this difference arose because luminance gain is greater locally for the dark band than for the light band, i.e., that it arose from a form of compressive luminance transduction, as we also suggest.

## Discussion

### Summary of the model’s main principles

We began with one main idea, that bars might be perceived at spatial peaks in the even-symmetric spatial filter output provided those peaks are not exceeded by the level of the odd filter output at the same place. Figure 11 shows in a single picture how that idea was applied and how it explains our findings. For a given stimulus scale ( $\sigma = 6$  min arc) we can approximate the multiscale model fairly well using a single filter scale ( $s = 6$  min arc) as we saw above. The odd filter is a Gaussian first-derivative, which both smooths the image and computes its derivative (gradient profile). The outcome  $E(x)$  is a smoothed derivative, shown as thin lines in Figure 11, for four values of the exponent ( $n = 1, 1.5, 2, 5$ ). Similarly, the even filter smooths and computes the second derivative of the image (the gradient of the gradient). The outputs  $B(x)$  are shown as thick curves in Figure 11, and their peaks—candidate bars—at positions  $x_0$  are marked by solid symbols.

We assumed that the ratio  $r = B(x_0)/E(x_0)$  was noisy, with variance  $v^2$  at scale  $\sigma$ , and that Mach bands would be seen on those occasions when the ratio  $r$  exceeded some criterion  $c$ . To visualize this noise in Figure 11, we can pretend that the odd filter is noise-free and attribute all the noise to the even filter. Thus the grey bars show  $\pm 1$  standard deviation of the noise, equal to  $v \cdot E(x_0)$  when expressed this way. The clear message is that for  $n = 1$  the candidate bar response lies well below the edge response and predicts 0% Mach bands, but as  $n$  increases the peak bar response rises and eventually

←

and light Mach bands (solid and dashed curves) along with data from Experiment 2, showing that fewer light Mach bands were marked (light triangles) than dark Mach bands (dark triangles). E: Like Figure 8B, a composite scale-space response map for Gaussian edge (Scale 6,  $n = 2$ ) but with nonlinear luminance response. Dashed white curve: nominal luminance profile. Solid white curve: luminance profile modified by front-end blurring and nonlinear transduction; note the leftward shift. F: as E, but exponent  $n = 5$ .

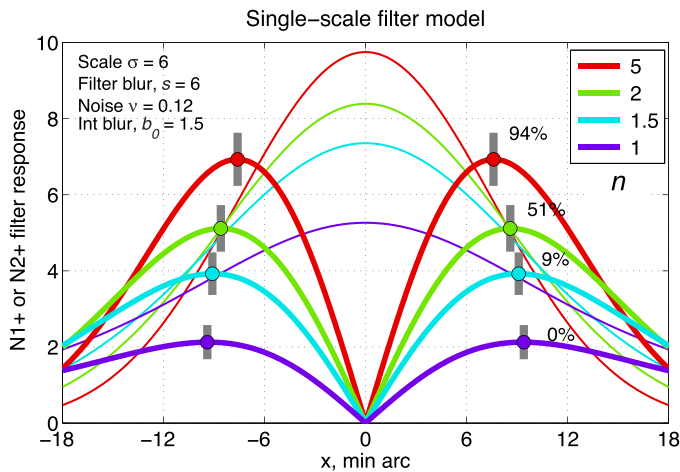


Figure 11. Summary of the main ideas developed in this paper, expressed at a single filter scale ( $s = 6$ ). Thin curves are the output of the odd filter in response to four of our edge images ( $n = 1$  to 5, as shown). Thick curves show the even (smoothed second derivative) filter output magnitude; peaks (filled circles) are candidate bars (Mach bands), and grey bars represent noise ( $\pm 1$  SD). Peaks in the even filter exceed the corresponding odd filter response more often with increasing  $n$ , thus predicting an increasing proportion of Mach bands (shown here as %), as observed in all three experiments. Locations of the peaks correctly predict perceived positions of Mach bands and the way they change with exponent  $n$  (Figure 5). See text for details.

exceeds the edge response quite reliably, giving 94% Mach bands for  $n = 5$ . This trend is similar to the experimental results (Figures 5B and 6). The mean Mach band position ( $\pm 8$  min arc) is also well described, as is the increase in separation of the bands as  $n$  decreases.

In short, in our model the emergence of Mach bands depends on the relation between the responses of even and odd spatial filters that have a suitable form (Gaussian first and second derivatives), with suitably chosen relative gains (influenced by parameters  $\alpha$ ,  $\beta$ ,  $k_1$ , Table 1) and a suitably selected spatial scale  $s$  for the filters. We see from Figure 11 that a single-scale model contains all the main elements for our proposed account of Mach bands, but automatic selection of spatial scale is a key advantage of the multiscale model, to which we now turn.

## The value of the multiscale model

We studied both the probability of observing Mach bands and the perceived spatial layout of the features of the bands (bars and edges) across a novel family of edge profiles. The results led to an apparent paradox for explanations based on the second spatial derivative of the luminance profile. On the one hand, the main factor determining Mach band probability was the exponent  $n$  that controls the sharpness of the corner in the

luminance profile. This main result (Figures 4 and 6) is similar to Ross et al.'s (1989) finding that contrast sensitivity for seeing Mach bands decreased markedly as the ramp was made more blurred. Blurring the ramp is analogous to decreasing  $n$ , and in both cases the second-derivative amplitude is correlated with corner sharpness and with Mach band perception. But, in apparent conflict with this idea, Experiments 1 and 3 showed that the likelihood of seeing Mach bands was largely independent of the spatial scale and image contrast in the suprathreshold range. These near-invariances imply that the probability of seeing Mach bands is not determined directly by the amplitude of peaks in the second derivative, because that is not invariant—it increases with image contrast and decreases greatly with increasing image scale (Figure 3).

This conflict was resolved by the multiscale model in two ways. First, we proposed that Mach bands (and presumably real bars too) depend on a comparison (the ratio) of the outputs of odd and even filters (Gaussian first and second derivatives, named E and B) at the peaks in the scale-space second derivative response. In agreement with our results, the model B:E ratio is contrast-invariant but increases with corner sharpness  $n$ . Second, the profound decrease in second derivative amplitude that would occur with increasing stimulus scale (Figure 3) is countered by the scale normalization factor ( $s^\beta$ , Equation 4). This key factor increasingly amplifies the response of the larger-scale filters. Importantly, the B:E ratio—and hence Mach bands—would be precisely scale-invariant as well as contrast-invariant, if  $s^\beta = s \cdot s^\alpha$ , implying  $\beta = \alpha + 1$ . This is because the second-derivative falls much faster than the first-derivative with increasing scale (inverse-square, vs. inverse), and so to maintain a constant B:E ratio, it needs to be amplified correspondingly more (by factor  $s$ ). Ideally then,  $\alpha = 0.5$  and  $\beta = 1.5$  (see Appendix 2). We set  $\alpha = 0.5$ , but found that  $\beta = 1.15$  (rather than 1.5) gave a better account of the data on Mach band layout, and this necessarily compromised the B:E scale invariance to a small extent that was compensated by allowing the criterion response ratio to differ at different stimulus scales. It would be more elegant if perfect scale invariance prevailed ( $\beta = 1.5$ ), but the data dictated otherwise.

To account for the edges of Mach bands that were otherwise hard to explain, we introduced a second process ( $E_2$ ) that is a nonlinear form of third derivative alongside the basic edge response (E) that is based on the first derivative. Such duplication is not implausible, but on grounds of parsimony, having two edge mechanisms might sound like one too many. We wonder whether some additional nonlinearity in the N3+ channel (Georgeson et al., 2007) might be able to unify the properties of E and  $E_2$  into a single edge mechanism, but this remains a task for future work.

## Comparison with other models

Many models of Mach bands have been proposed (Pessoa, 1996) having many common features (Kingdom & Moulden, 1992; Morgan, 2011). It is difficult to rule out any model completely, because every model is really a class of models that are variants of each other with different parameters and different ancillary assumptions. Even if all tested versions fail, some modified version as yet untested might succeed. And useful insights may be drawn from several related models, even though none is perfect. From such ideas new information-theoretic methods of *multimodel inference* have been developed (Burnham & Anderson, 2004). Full evaluation of other models is beyond the scope of this paper, but some brief comments are in order.

The properties of the MIRAGE model (Watt & Morgan, 1985) are well-known and it has several points of contact with ours. It uses linear, even-symmetric (Gaussian second derivative) filters at several scales and half-wave rectifies the outputs to give responses very like  $B^+$  and  $B^-$  in the present model; then it combines outputs of the same sign across scales and uses a fixed set of rules to interpret the two resulting profiles as features. In brief, if two adjacent peaks of the combined responses have opposite signs they are interpreted as an edge, but if those two peaks are separated by a gap (a null region in the filter responses) then the two peaks would be interpreted as a pair of light and dark bars. The response to a Mach ramp is of the latter kind, giving two bars as the output description. This rule works well for Mach ramps (high  $n$ ), but it cannot predict Mach bands on a Gaussian edge, because no null region exists between the peak and trough in this case at any one filter scale or in the combined response. Our experiments consistently showed Mach bands to be reported on about 60% of trials for Gaussian edges ( $n = 2$ ), and this does not appear to be a baseline rate of false alarms or guesses because much lower probabilities were recorded for  $n = 1.5$  and  $n = 1$ . Thus, without modification, MIRAGE cannot predict the Mach bands seen on Gaussian edges. Indeed the two interpretations (as one edge or two bars) are mutually exclusive; unlike the present model, MIRAGE could never see Mach bands and an edge at the same time. This is evidence against the enforced combination of responses across filter scale, as Kingdom and Moulden (1992, p. 1579) pointed out.

Ross et al. (1989) described other difficulties for MIRAGE, and they claimed that it did not mark Mach bands for ramp widths of 25 min arc wide or less. This was inconsistent with their results (and indeed with our results, given that our ramp width,  $2\sigma$  for high  $n$ , was always less than 25 min arc). However, our own simulations of MIRAGE confirmed the original report of Watt and Morgan (1985), reiterated by Morgan and

Watt (1997), that MIRAGE does deliver Mach bands for ramps as narrow as 5 min arc. We found that this depended on a suitable choice of the model's noise-reduction threshold. Thus the apparently conflicting predictions derived from the same model may hinge on details of implementation—an example of the difficulty of model comparison referred to above. When we applied MIRAGE to our stimulus set we confirmed that no Mach bands were predicted for  $n \leq 2$ , and we could not find any set of parameters that would consistently deliver Mach bands at all three stimulus scales (3, 6, and 12 min arc).

Kingdom and Moulden's (1992) MIDAAS model was a development of MIRAGE, and it aimed to explain the (often illusory) profiles of perceived brightness for a wide range of 1-D luminance profiles, conceiving of brightness as a continuous function over space. This contrasts with feature detection models, including the present one, which aim to derive a sparse set of features describing the spatial structure of the luminance profile (see review by Morgan, 2011). Ideally, a model of early spatial vision would do both; our model is limited at present because it has little to say about apparent brightness either at feature locations or between them. MIDAAS is successful, at least qualitatively, in accounting for a wide range of brightness phenomena though it has not, as far as we know, been tested quantitatively on available datasets. And although it uses the MIRAGE edge/bar parsing rules at each filter scale as a step towards deriving brightness, it does not appear to deliver a feature description after the outputs at different filter scales have been combined (averaged) to produce the final brightness profile. Hence it is not clear that it could be tested against our present dataset.

The local energy model (Morrone & Burr, 1988) predicts the occurrence of light and dark bars from peaks of energy on Mach ramps, and with some ancillary assumptions about the processes of detection, it successfully predicted contrast thresholds for seeing Mach bands and the increase in these thresholds as the ramp was made more blurred (Ross et al., 1989). But du Buf (1994; figure 14) showed that very similar predictions could be obtained from the even-symmetric filters alone without combining even and odd responses into an energy measure.

Our efforts to predict the observed Mach band positions (Figure 5J, K, L) from peaks of local energy met with only limited success. We implemented the filters from the description given by Ross et al. (1989) but allowed a broad range of filter scales so that we could examine the behavior of energy peaks over scale. For  $n \leq 2$ , no Mach bands appeared; instead, at all filter scales, a single energy peak represented only the central edge. For  $n = 3$  to 5, Mach bands of the correct polarity appeared across a range of filter scales, but

their positions varied smoothly with filter scale and without a rule for scale selection we could not properly compare those positions with our data. For the sine edge, Mach bands were predicted only over a narrow range of filter scales. At finer scales the energy model instead incorrectly reported edges (not bars) located at  $x = \pm h / 2$ , where  $h$  is the width (half-period) of the sine edge—an effect that arises from discontinuity in the higher spatial derivatives at these two locations. To screen out these false edges a rule for scale selection would again be needed. In short, the energy model does predict Mach bands, but would need modification to be tested against our results. As with MIRAGE, it is possible that some new assumptions about scale selection, filter bandwidth, or other changes of implementation detail might improve it.

More generally, it is well known that the energy model suffers what du Buf (1994, p. 458) called the “curse of the sinewave grating”—that no features are predicted for a periodic sinewave luminance profile, while human observers clearly see light and dark bars and can judge the position and blur of the edges between them (Georgeson et al., 2007). This curse is intrinsic to the energy model: For any luminance waveform the local energy profile is, by definition, the envelope of the outputs of the paired quadrature-phase filters and that smooth envelope has no peaks at many of the underlying features that humans perceive (Hesse & Georgeson, 2005).

The present model aimed to draw insight from these earlier models and others while overcoming some of the problems just discussed. (a) Unlike MIRAGE, it uses the outputs from filters at particular scales rather than combining them across scales. But it does not allow arbitrary access to different filter scales and positions; instead it uses scale normalization and peak-finding in scale-space (Figures 8, A1, A2) to reduce the response maps to a sparse set of feature points whose scale and location are given by the peak point and whose identity (bar or edge) and polarity is given by the identity of the map ( $B^\pm$  or  $E^\pm$ ) in which the peak occurs. (b) Like the energy model, but unlike MIRAGE, it compares even and odd filter responses to classify bars and edges respectively, but the manner of comparison is different from the energy model. Both use the B/E ratio, but rather than using the ratio at energy peaks as a measure of local phase, our model uses the ratio as an indication that a peak bar response B should be treated as significant.

One key difference between models is whether they adopt spatial filters that have only even symmetry (MIRAGE; MIDAAS) or parallel filters with even and odd symmetry (energy model; the present model). Physiological evidence tends to favor the idea that V1 cell receptive fields come with a wide range of symmetries (phase characteristics) including even and odd (e.g., Field & Tolhurst, 1986; Hamilton, Albrecht

& Geisler, 1989) with some preference for even and odd over intermediate phases (Ringach, 2002). In psychophysics, Huang, Kingdom, and Hess (2006) failed to replicate one of the key studies that implicate distinct even and odd filters in spatial vision tasks (Burr, Morrone, & Spinelli, 1989) and proposed instead that psychophysical phase discrimination tasks are based solely on even-symmetric filters. This pivotal issue needs further study.

## Conclusion

The multiscale Gaussian-derivative model (N2+I+) developed here is related to several earlier models, and gives an accurate, principled, and detailed account of the appearance of bar and edge features in Mach bands over a range of scales and spatial waveforms. It needs to be tested over a broader range of stimulus types and will no doubt need further development, but it holds promise as the basis for a more general theory of feature coding in human vision.

## Acknowledgments

SAW was supported by an EPSRC doctoral training grant to Aston University, and this work was supported in part by BBSRC grant BB/H00159X/1 to Mark Georgeson and Tim Meese.

Commercial relationships: none.

Corresponding author: Stuart A. Wallis.

Email: s.a.wallis2@aston.ac.uk.

Address: School of Life and Health Sciences, Aston University, Birmingham, UK.

## References

- Burnham, K. P., & Anderson, D. R. (2004). Multi-model inference: Understanding AIC and BIC in model selection. *Sociological Methods Research*, 33, 261–304.
- Burnham, R. W., & Jackson, J. E. (1955). Mach rings verified by numerical differentiation. *Science*, 122, 951–953.
- Burr, D. C., Morrone, M. C., & Spinelli, D. (1989). Evidence for edge and bar detectors in human vision. *Vision Research*, 29, 419–431.
- Campbell, F. W., & Robson, J. G. (1968). Application of Fourier analysis to the visibility of gratings. *The Journal of Physiology*, 197, 551–566.

- Charman, W. N., & Watrasiewicz, B. M. (1964). Mach effect associated with microscope images. *Journal of the Optical Society of America*, *54*, 791–794.
- du Buf, J. M. H. (1994). Ramp edges, Mach bands, and the functional significance of the simple cell assembly. *Biological Cybernetics*, *70*, 449–461.
- Field, D. J., & Tolhurst, D. J. (1986). The structure and symmetry of simple-cell receptive-field profiles in the cat's visual cortex. *Proceedings of the Royal Society of London B*, *228*, 379–400.
- Foley, J. M., & Legge, G. E. (1981). Contrast detection and near-threshold discrimination in human vision. *Vision Research*, *21*, 1041–1053.
- Georgeson, M. A. (1987). Temporal properties of spatial contrast vision. *Vision Research*, *27*, 765–780.
- Georgeson, M. A., & Sullivan, G. D. (1975). Contrast constancy: Deblurring in human vision by spatial frequency channels. *The Journal of Physiology*, *252*, 627–656.
- Georgeson, M. A., & Freeman, T. C. A. (1997). Perceived location of bars and edges in one-dimensional images: Computational models and human vision. *Vision Research*, *37*, 127–142.
- Georgeson, M. A., May, K. A., Freeman, T. C. A., & Hesse, G. S. (2007). From filters to features: Scale-space analysis of edge and blur coding in human vision. *Journal of Vision*, *7*(13):7, 1–21, <http://www.journalofvision.org/content/7/13/7>, doi:10.1167/7.13.7.
- Georgeson, M. A., & Turner, R. S. E. (1985). Afterimages of sinusoidal, square-wave and compound gratings. *Vision Research*, *25*, 1709–1720.
- Hamilton, D. B., Albrecht, D. G., & Geisler, W. S. (1989). Visual cortical receptive fields in monkey and cat: Spatial and temporal phase transfer function. *Vision Research*, *29*, 1285–1308.
- Heeger, D. J. (1992). Half-squaring in responses of cat striate cells. *Visual Neuroscience*, *9*(5), 427–443.
- Helmholtz, H. (2000). *Treatise on Physiological Optics* (Vol. 2). (J. P. C. Southall, Trans.). Bristol: Thoemmes Press. (Original work published 1867).
- Hesse, G. S., & Georgeson, M. A. (2005). Edges and bars: Where do people see features in 1-D images? *Vision Research*, *45*, 507–525.
- Huang, P. C., Kingdom, F. A. A., & Hess, R. F. (2006). Only two phase mechanisms,  $\pm$ cosine, in human vision. *Vision Research*, *46*, 2069–2081.
- Kingdom, F., & Moulden, B. (1992). A multi-channel approach to brightness coding. *Vision Research*, *32*, 1565–1582.
- Koenderink, J. J. (1984). The structure of images. *Biological Cybernetics*, *50*, 363–370.
- Koenderink, J. J., & van Doorn, A. J. (1987). Representation of local geometry in the visual-system. *Biological Cybernetics*, *55*, 367–375.
- Legge, G. E. (1978). Sustained and transient mechanisms in human vision: Temporal and spatial properties. *Vision Research*, *18*, 69–81.
- Legge, G. E., & Foley, J. M. (1980). Contrast masking in human vision. *Journal of the Optical Society of America*, *70*, 1458–1471.
- Lindeberg, T. (1998). Edge detection and ridge detection with automatic scale selection. *International Journal of Computer Vision*, *30*, 117–154.
- Lindeberg, T. (1994). *Scale-space theory in computer vision*. Dordrecht: Kluwer.
- Ludvigh, E. (1953a). *Perception of contour: I. Introduction*. (Report No. NM 001 075.01.04). Pensacola, FL: US Naval School of Aviation Medicine, <http://www.dtic.mil/dtic/tr/fulltext/u2/019386.pdf>.
- Ludvigh, E. (1953b). *Perception of contour: II. Effect of rate of change of retinal intensity gradient*. (Report No. NM 001 075.01.05). Pensacola, FL: US Naval School of Aviation Medicine, <http://handle.dtic.mil/100.2/AD0019384>.
- Mach, E. (1865). *On the effect of the spatial distribution of the light stimulus on the retina*. In F. Ratliff (Ed.) *Mach Bands: Quantitative Studies on Neural Networks in the Retina* (pp. 253–271).
- Mather, G., & Morgan, M. (1986). Irradiation - implications for theories of edge localization. *Vision Research*, *26*, 1007–1015.
- Morgan, M. (2011). Features and the 'primal sketch'. *Vision Research*, *51*, 738–753.
- Morgan, M. J., & Watt, R. J. (1997). The combination of filters in early spatial vision: A retrospective analysis of the MIRAGE model. *Perception*, *26*, 1073–1088.
- Morrone, M. C., & Burr, D. C. (1988). Feature detection in human vision - a phase-dependent energy model. *Proceedings of the Royal Society of London Series B - Biological Sciences*, *235*, 221–245.
- Nachmias, J., & Sansbury, R. V. (1974). Grating contrast - discrimination may be better than detection. *Vision Research*, *14*(10), 1039–1042.
- O'Brien, V. (1958). Contour perception, illusion and reality. *Journal of the Optical Society of America*, *48*, 112–119.
- Pessoa, L. (1996). Mach bands: How many models are possible? Recent experimental findings and modeling attempts. *Vision Research*, *36*, 3205–3227.

- Ratliff, F. (1965). *Mach bands: Quantitative studies on neural networks in the retina*. San Francisco: Holden-Day.
- Ringach, D. (2002). Spatial structure and symmetry of simple-cell receptive fields in macaque primary visual cortex. *Journal of Neurophysiology*, *88*, 455–463.
- Ross, J., Holt, J. J., & Johnstone, J. R. (1981). High frequency limitations on Mach bands. *Vision Research*, *21*, 1165–1167.
- Ross, J., Morrone, M. C., & Burr, D. C. (1989). The conditions under which Mach bands are visible. *Vision Research*, *29*, 699–715.
- ter Haar Romeny, B. M. (2003). *Front-end vision and multi-scale image analysis*. Berlin: Springer.
- Thomas, J. P. (1965). Threshold measurements of Mach bands. *Journal of the Optical Society of America*, *55*, 521–524.
- Wallis, S. A., & Georgeson, M. A. (2009). Mach edges: Local features predicted by 3rd derivative spatial filtering. *Vision Research*, *49*, 1886–1893.
- Watson, A. B., & Ahumada, A. J. (2011). Blur clarified: A review and synthesis of blur discrimination. *Journal of Vision*, *11*(5):10, 1–23, <http://www.journalofvision.org/content/11/5/10>, doi:10.1167/11.5.10. [PubMed] [Article]
- Watt, R. J., & Morgan, M. J. (1985). A theory of the primitive spatial code in human vision. *Vision Research*, *25*, 1661–1674.
- Weale, R. A. (1979). Discoverers of Mach bands. *Investigative Ophthalmology & Visual Science*, *18*(6), 652–654, <http://www.iovs.org/content/18/6/652>. [PubMed] [Article]

## Appendix 1. Parsing rules applied to the feature-marking data

The parsing rules were applied to the data from each condition in turn and consisted of two passes over the data as follows (for light-to-dark images, LD):

First Pass:

1. Obtain the data for one trial.
2. If there are seven features, place each one in the seven bins, in position order.
3. If there are fewer than seven features, then:
  - a. Place any bars into the bar bin of its polarity (Bins 2 and 6).
  - b. Place any DL edges that are to the left of the image center in Bin 1.
  - c. Place any DL edges that are to the right of the image center in Bin 7.
  - d. If there are three LD edges, place them in Bins 3 to 5, in position order, but if there are less than three then delay assignment until second pass.
4. Repeat the above steps for every trial in the same condition.

Second Pass:

1. Calculate the position of each bin from the mean of its contents.
2. Obtain all of the LD data remaining from Pass 1 for the whole condition, and place each datum in its nearest LD bin.
3. Recalculate the LD bin positions from the mean of their contents.

Finally, the mean position of each feature was assigned as the mean of each bin's contents.

## Appendix 2. Scale space response maps from the N2+1+ model

The edge mechanism has odd-symmetric, Gaussian first-derivative filters—described as model N1 (mnemonic: N for scale-normalized, 1 for first-derivative) by Georgeson et al. (2007). Half-wave rectification of its outputs creates separate channels for positive and negative edges, N1+ and N1-. That model is extended here to include a parallel system of even-symmetric, Gaussian second-derivative, bar-sensitive channels (N2+) whose definition is exactly analogous to N1+. The combined model is called N2+1+. When the E<sub>2</sub> process is added, we refer to “the full N2+1+ model.”

### Examples

An example of the scale-space bar maps alone (B<sup>+</sup> and B<sup>-</sup>) is shown in Figure A1(A) in response to two Gaussian bars of different scales. The corresponding edge maps alone (E<sup>+</sup> and E<sup>-</sup>) are in Figure A1(B). Since all responses are positive, a convenient way to visualize the population response is to plot a single map,  $M(x, s) = \max(E^+, E^-, B^+, B^-)$  where the max operator picks the largest of the four responses at each position and scale  $(x, s)$ . The composite map  $M(x, s)$  for the same two bars (Figure A1(C)) shows how the relation between E and B responses may be important in deciding what features are present. Potential Mach bands (blue squares in Figure A1(A)) may be occluded by larger edge responses (E<sup>+</sup> or E<sup>-</sup>) at the same place and might not be visible (squares now shown as open

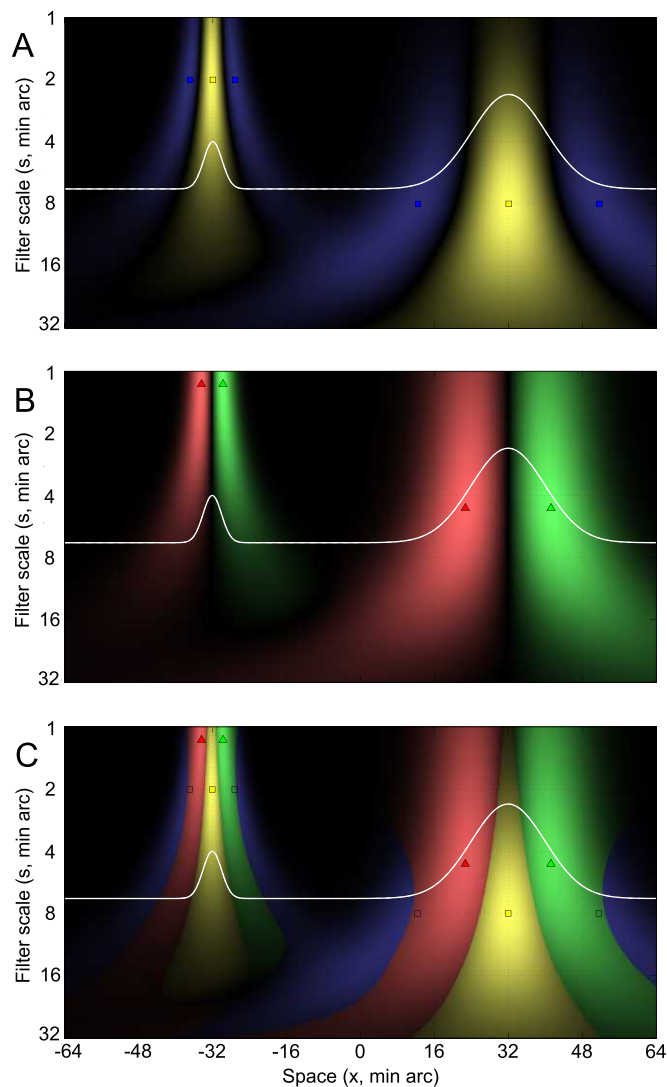


Figure A1. A: Scale-space map of the second-derivative N2+ channel responses ( $B^+$ , yellow;  $B^-$ , blue) to two Gaussian bars of scales 2 and 8 min arc. White trace is their luminance profile. Peak B responses are marked by square symbols. Note that the bar positions ( $\pm 32$  min arc) and scales (2, 8 min arc) are veridically encoded (two yellow squares) but there are potential Mach bands (dark bars; blue square symbols) flanking each light bar. B: Map of the first derivative N1+ channel responses ( $E^+$ , red;  $E^-$ , green) to the same two Gaussian bars. C: All four channel responses together. This map is a composite of Panels A and B and shows only the largest of the four responses at each scale-space point. Peak B responses are marked by squares, peak E responses by triangles. Amplitude scaling (normalization) exponents were chosen to give scale invariance:  $\alpha = 0.5$ ,  $\beta = 1.5$ ; see [Appendix](#) for details.

symbols in [Figure A1\[C\]](#)), depending on noise and decision factors discussed in the main text.

A similar analysis for input comprising two Gaussian edges of different blurs is given in [Figure A2](#). Note how the potential Mach bands (open squares) might be occluded by the E response (pink region).

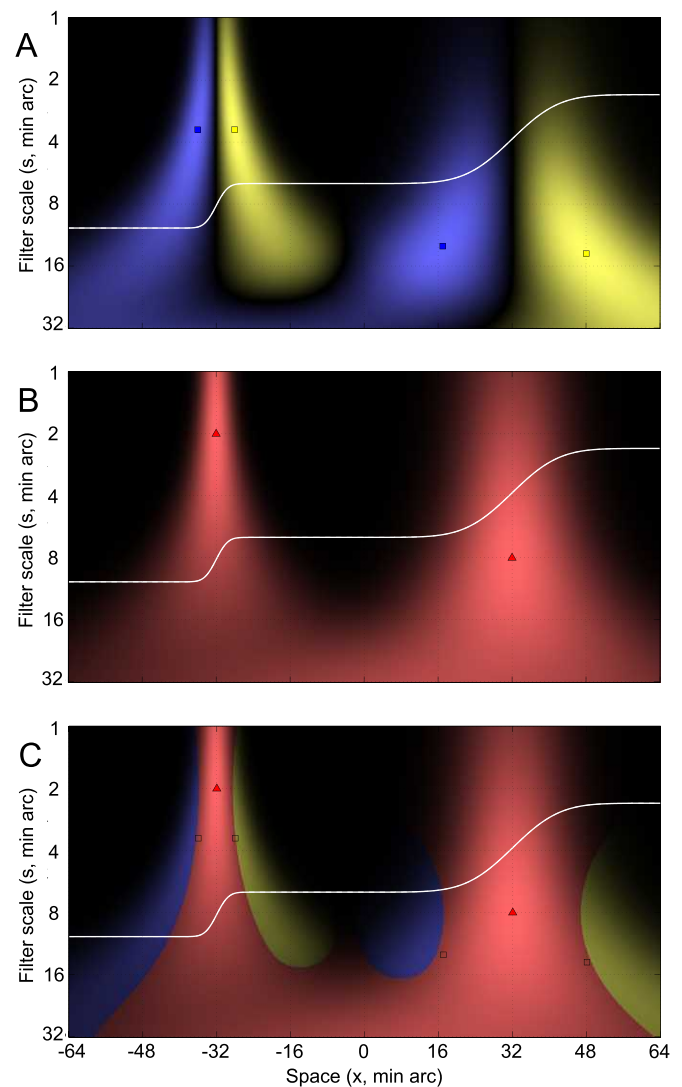


Figure A2. A, B, and C: As [Figure A1](#), but for two Gaussian-blurred edges ( $n = 2$ ), again with blurs of 2 and 8 min arc. Peak responses are marked by symbols. Note that edge positions ( $\pm 32$  min arc) and scales (2, 8) are veridically encoded (two red triangles) but there are potential Mach bands (light or dark bars; square symbols) flanking each edge.

With scaling exponents  $\alpha = 0.5$ ,  $\beta = 1.5$ , the relative activation of E and B filters and the relative scales and positions of bar and edge features are all scale-invariant. Despite these elegant properties, we found that that this scale invariance property did not hold exactly when the experimental data were fitted; we had to reduce  $\beta$  to about 1.15 to match the observed spatial layout of Mach bands shown in [Figure 5](#), thus compromising this scale invariance to some extent.